NTNU – Trondheim
Norwegian University of
Science and Technology

Synthesis of ilmenite

Vincent Yves Canaguier

Materials Science and Engineering
Submission date: June 2014
Supervisor: Leiv Kolbeinsen, IMTE
Co-supervisor: Stian Seim, TTI Norway
Stephen Lobo, IMTE

Norwegian University of Science and Technology
Department of Materials Science and Engineering

Preface

This Master's Thesis has been carried out at the Department of Material Science and Engineering at the Norwegian University of Science and Technology during the spring semester of 2014. The project was done in cooperation with TiZir Titanium & Iron AS in Tyssedal. The idea was brought up by the need of a pure ilmenite of reference in order to investigate the impurities effect in ilmenite ores.

Trondheim, 2014-06-16

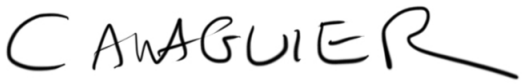

Vincent Canaguier

Acknowledgment

I would like to thank the following persons for their help during this Master's Thesis:

First, I would like to thank Professor Leiv Kolbeinsen for his help and weekly discussions, for approximately one year during a summer job, the Master's Project and the present Master's Thesis.

I would also like to thank Stephen Lobo, for his explanations and his time. His advices about the technical aspects and the scientific work in general were precious.

Stian Seim is also greatly acknowledged for his advices and help during the Thesis. It has been a pleasure to visit Tyssedal plant again this semester.

Delphine Leroy is also thanked for her time and support to get the cold crucible induction furnace ready.

I would also like to thank Julian Tolchard and Morten Peder Raane for their help for the analysis.

Edith Thomassen and Trygve Schanche are gratefully acknowledged for their help with the pellets and samples preparation.

Finally, I would like to thank Merete Tangstad and the whole SiManTi Group for the various trainings, the valuable feedback and the fun.

V.C.

Abstract

Ilmenite ores are currently processed at TiZir Titanium & Iron AS in Tyssedal. To be prepared for a change in the raw material composition, the effect of the impurities in the ilmenite ores has to be investigated. It is particularly important to know the behavior of these impurities during the reduction processes. Thus, a synthesis method to produce a pure raw material of reference has to be developed in a reproducible way. This works also focuses on the addition of chosen impurities in the ilmenite synthesized. Ultimately, the reduction reactions are investigated.

The synthesis of pure ilmenite is developed using the cold crucible induction furnace. A melting route is used for both pure ilmenite and Mg-rich ilmenite synthesis with iron, iron oxide, titanium oxide and magnesium oxide as starting materials. Two gas reduction experiments have been carried out, using CO and H_2 gas. Mass loss curves, XRD analysis and electron probe micro-analysis are obtained from these experiments.

The pure and Mg-rich ilmenite synthesized correspond to the expectations, showing only a few of undesired phases. Potential improvements for the process are also given, concerning in particular the raw materials positioning in the crucible. The reduction experiments show three distinct steps in the case of H_2 reduction, but only two with CO. The results suggest that the particle size might be determining for the CO reduction. The stopping of the experiment by cutting the reducing gas flow is proposed to investigate the reaction closer.

Contents

List of Figures

List of Tables

Chapter 1

Introduction

This chapter will present aspects related to the motivation of the thesis, the objectives and their limitations and a summary of the present work.

1.1 Background

Problem formulation

The aim of this thesis is to increase the knowledge of ilmenite processing. Ilmenite is indeed not a widely known material due to its limited use is today's industry. In fact, the ilmenite ore production is about five hundred times less important than the iron ore production (U.S. Geological Survey, 2013). Moreover, ilmenite is not pure in its natural state and various ilmenite types differ in their composition, regarding the impurities and their concentration. A major question is the influence of these impurities on the ore's behavior while processed. This is particularly important in order to be prepared for a change of raw materials in an existing process because of a deposit getting depleted. To be able to gather new information, studies on specific compositions of ilmenite ore would be a step forward in the understanding of the impurities effect. A first aspect of this work is the synthesis of a pure ilmenite of reference which could be used for further experiments. This task has been previously partly carried out by the author during a master project (Canaguier, 2013b) and is here extended. Furthermore, reduction experiments on pure ilmenite have been done to initiate the use of the new material produced and investigate the reduction mechanisms. Finally, a synthesis route to produce ilmenite with a controlled amount of specific impurity (Mg) has been developed.

Literature survey

The present work has been developed thanks to various other works. The ilmenite synthesis technique by melting was developed using the results from Borowiec and Rosenqvist which provided most of the knowledge on the Fe-Ti-O system and on the Fe-Ti-Mg-O system. This knowledge has also been addressed in the works of Grey, Jones and Reid. Their articles were essential for the ilmenite gaseous reduction understanding. Additional works from Vijay, Hussein and others developed the knowedge of the author on the processes during reduction, and the work from Lobo particularly gave a accurate insight of the mechanisms involved. The choice of the equipment was influenced by the works of Seim and Pistorius for the synthesis part, and Lobo for the reduction. Finally, the understanding of the shrinking core model was provided by the work of Levenspiel. Other documents and works have been used by the author and will be referenced in the relevant sections.

1.2 Objectives

The main objectives of this Master Thesis are:

1. To develop a reproducible process for pure ilmenite synthesis fitting the requirements of further laboratory uses.

2. To investigate the synthesis of a $FeTiO_3$-$MgTiO_3$ solid solution with a controlled amount of Mg.

3. To investigate the reduction processes of pure ilmenite, particularly in terms of speed and extent.

1.3 Scope

Concerning the production of synthetic ilmenite, the requirements in terms of purity are not quantitative. Although a majority of the product has to be ilmenite to be called as such, the presence of other phases is accepted to some extent. Concerning the gaseous reduction work, a deepened explaination of the process is not expected from this work.

Nevertheless, the production of data as well as an analysis providing clues on the mechanisms and propositions for further investigations is expected.

1.4 Approach

The synthesis of ilmenite initiated during another work by the author is to be improved. By drawing the conclusion of the previous work (Canaguier, 2013b), new experimental parameters are varied, for example the power supply. Ultimately, analysis by XRD is used to confirm that both the product and the process fit the expectations.

Concerning the gaseous reduction, the experiments have to be done in a similar way to the experiments carried by Lobo (Lobo et al.). The present results are to be used as an input for other works and must be comparable.

Finally, the Mg-rich ilmenite synthesis is to be developed empirically. Given that this synthesis is at an early level of development, the approach is to test the first assumptions on the effect of several parameters.

1.5 Structure of the report

The rest of the report is structured as follows.

Chapter 2 gives the background of ilmenite synthesis and processing, from the synthesis in nature and the existing synthesis techniques in laboratory to the processing in the industry.

Chapter 3 provides the knowledge gathered on the subject of the thesis through a litterature survey. This knowledge applies to the ilmenite synthesis, to the Mg-rich ilmenite synthesis and the gaseous ilmenite reduction.

Chapter 4 describes the experiments carried out by the author, as well as the analysis done at various stages.

Chapter 5 details the results obtained during the experiments and analyses. Both qualitative and quantitative results are given.

Chapter 6 discusses the results looking at the theory elements provided before, as well as other works findings. Possible explainations on the mechanisms are also given.

Chapter 2

Background

2.1 Ilmenite in nature

Natural synthesis of ilmenite

The synthesis of ilmenite in nature is a standing debate. Many mechanisms have been proposed, and some are also disproved. Moreover, the ilmenite synthesis is often more a combination of several mechanisms than simply modeled after only one process. It is also highly dependent of each deposit and different mechanisms take place in different areas.

An early study reports the forming of oxide-apatite rocks containing both magnetite and ilmenite (Philpotts, 1967). In particular, it also reported findings on crystallization temperature of iron-titanium-oxide apatite rocks. According to the paper, the range of crystallization is around 850°C to 1000°C, and the melt is obtained by immiscibility mechanisms from a silica melt. However, new evidence disproves the previous results (Lindsley, 2003). In fact, Lindsley notes that the temperature during the experiments carried by Philpotts, 1400°C, is too high for crustal conditions. In addition, attempts to produce such melts in laboratory at reasonable temperature conditions failed to prove the immiscibility mechanisms. A study on Panzhihua intrusions also goes in favor of an early crystallization of Fe-Ti oxide phase from the magma rather than a liquid segregation (Pang et al., 2008).

Other mechanisms explain the composition and formation of ilmenite deposits like, for example, the Tellnes deposit. A recent publication explains the four main factors involved (Charlier et al., 2007): fractional crystallization, liquidus mineralogy, trapped

liquid fraction and post cumulus re-equilibration. These mechanisms, together, provide information on how the composition varies during crystallization.

Other works (Charlier et al., 2006) reports the pressure condition during crystallization to be around 5 kbar. By analyzing a known crystallization path of similar composition while varying the pressure, Charlier concluded that 5 kbar fits the crystallization sequence observed in Tellnes.

To conclude, many mechanisms have been proposed to explain the forming of ilmenite in different rocks. Given that an impossibility of an immiscibility mechanism is supported by experimental evidences (Lindsley, 2003), a separation of Fe-Ti oxides on a solid form is more likely to have occurred. Other mechanisms help to explain how the different compositions were obtained. Moreover the 5 kbar value is agreed by many papers, as reported by Charlier and Lindsley (Charlier et al., 2007; Lindsley, 2003). Likewise, temperatures lower than 1000°C are agreed to be more likely to occur in the crust.

Origin of the impurities in natural ilmenite

The study on Panzhihua intrusions (Pang et al., 2008) also gives information on how some species are exchanged between minerals. This helps to explain the impurity content after cooling of the rock, especially the Mg content in these rocks. Of course these mechanisms depend on the original magma composition and crystallization and cannot be applied to any ilmenite ore. Kwan-Nang Pang also argues that these re-equilibration mechanisms help at the forming of ilmenite. The different reactions of inter-oxide re-equilibration that are pointed out in this paper are as shown in Equations 2.1- 2.4:

$$Fe_2TiO_4(\text{in magnetite}) + Fe_2O_3(\text{in ilmenite}) = FeTiO_3(\text{in ilmenite}) + Fe_3O_4(\text{in magnetite}) \quad (2.1)$$

$$Mg^{2+}(\text{in magnetite}) + Fe^{2+}(\text{in ilmenite}) = Mg^{2+}(\text{in ilmenite}) + Fe^{2+}(\text{in magnetite}) \quad (2.2)$$

$$6Fe_2TiO_4(\text{in magnetite}) + O_2 = 6FeTiO_3(\text{ilmenite}) + 2Fe_3O_4(\text{in magnetite}) \tag{2.3}$$

$$6Fe_2TiO_4(\text{in magnetite}) + CO_2(\text{fluid}) = 6FeTiO_3(\text{ilmenite}) + 2Fe_3O_4(\text{magnetite}) + C(\text{graphite}) \tag{2.4}$$

All these reactions go to the right with decreasing temperature. Due to Equation 2.1, ilmenite and magnetite go towards their end composition, i.e. $FeTiO_3$ and Fe_3O_4. The second reaction, in Equation 2.2, expresses the Mg transfer from the magnetite phase to the ilmenite one. These two reactions respectively happen between 500-650°C and 460-680°C according to Kwan-Nang Pang. Reaction Equation 2.3 occurred in Panzhihua intrusions because of the rocks where the magma was emplaced. Another way to write this reaction is given in Equation 2.4. In fact, the limestone originally present provided CO_2 for the reaction. The reaction's temperature is found to be around 700°C.

Summary

Rocks containing ilmenite in nature are the result of complicated reactions and processes. Examples of possible mechanisms have been given above, but these are only some of the processes proposed. Even though information has been found on the forming conditions, like temperature or pressure, a fully explained mechanism has not been found. Moreover, all these finding are strongly dependent of each intrusion and no general process was determined.

2.2 Existing synthesis techniques

In an early work by the author, numerous synthesis techniques have been reported (Canaguier, 2013a). These techniques have been used for many purposes more or less close to the present needs. A summary of these techniques as well as their main features is given in Table 2.1.

Table 2.1: Various synthesis processes and their caracteristics (Canaguier, 2013a).

Synthesis technique	Maximum temperatures involved	Grain/ Crystallite size	Time needed	Advantages	Drawbacks
Coprecipitation procedure	100°C	100 nm	Fast process		Additional condition on cations
Digestion method	300°C	100 nm	Time costly		Formation of carbonates
Citrate gel technique	400°C	70 nm		Simple procedure	
Citrate gel technique with surfactant	600°C	25 nm		Homogeneity Composition control	
Novel liquid mix and H_2/H_2O reduction	600°C	76 nm	Time costly (24h drying)	Simple/Cheap procedure	Not so common
Cristal growth of $FeTiO_3$	1415°C	-		Single Crystal	Over quality
Dry synthesis (vacuum)	930°C	45 nm*		Common	
Dry synthesis (argon)	1200°C	-	-		Not much information
Synthesis in alcohol	1100°C		Time costly (25h heating)		Few explanations
Synthesis in a solar furnace	2000°C	-	Fast process	May lead to another technique	

*Authors guess by drawing a parallel with the size obtained for $NiTiO_3$. The analogy may not be viable.

Two types of synthesis techniques have been pointed out: chemical routes and metallurgical routes. The chemical routes usually need lower temperatures and a controlled grain size. However, the processes are not intuitive and require complex compounds. In addition, the quantities produced might not be fitting the requirements. The metallurgical routes proposed require raw materials simplier to handle, such as TiO_2, Fe and Fe_2O_3. However, the time needed for these syntheses is sometimes long, which does not help an empirical development of the technique.

2.3 About the Tyssedal process

In this section, the process carried out at Tyssedal by TiZir Titanium & Iron AS is explained. This process is a key part of the thesis since the focus is to investigate ilmenite's properties and thus create knowledge in this field. This part has been written using the documentation from Solheim and Folmo (Solheim, 1988; Folmo and Rierson, 1992).

Raw materials origin

The ilmenite ore processed at Tyssedal plant is obtained from Tellnes mine, in Norway. The ore itself contains 18% TiO_2 before any treatment. The ore is next enriched in TiO_2 content using flotation and gravity separation, which brings the content to 44.6% TiO_2. This enriched ore composition is reported and presented in Table 2.2.

Table 2.2: Tellnes ore analysis (Solheim, 1988).

Oxides	Proportions in Tellnes Ore
$\%TiO_2$	44.6
%FeO	34.8
% FeO_3	11.9
% SiO_2	2.8
%MgO	4.7
% Al_2O_3	0.7
$\%Cr_2O_3$	0.07

However, this ore is not the only one to be processed in Tyssedal. Actually, the Grande Côte mineral sand project developed by TiZir aims at producing a new raw material from ilmenite rich sands (Ackland, 2011). Of course, the impurities will be slightly different in the two raw materials.

Raw materials preparation

According to Solheim and Folmo, the ilmenite is first milled to the appropriate size prior to being pelletized. This milled material is then dried up to 9% of moisture to form filter cakes using a vacuum filter. These cakes are then mixed with the binder, which here is bentonite. The bentonite content is set to be 0.8% according to Solheim. Folmo reports that 7.5 kg of bentonite is added to each ton of filter cake, which would make it 0.744% bentonite. In a pelletizing drum, the pellets are shaped. The size of the pellets is in the range 9-16mm. Small seeds and oversized green pellets are separated from the finished ones to be recycled and reprocessed in a second run.

Hardening and oxidizing of the pellets

After the green pellets are produced, they are introduced on the travelling grate. The aim here is to process the pellets with a heat treatment in order to harden them. Without such a treatment, the pellets would fall to pieces because of the shocks in the rotary kiln. In the travelling grate, exhaust gas from the rotary kiln is used. The green pellet bed is thus heated up to 750°C in oxidizing conditions, for a total duration of about 20 minutes.

Pre-reduction and partial metallization

The hardened pellets are then charged in the rotary kiln with reduction materials. The pieces of coal, whose size is between 3 and 25 mm, aimed at providing the reducing conditions as well as the heating. The pellets are partly reacted up to a metallization degree between 70 and 75%. The pellets and reduction materials are kept in the rotary kiln for 9 hours with a rotation speed of 0.5 rpm at a temperature of 1150°C. The partly reduced product is then charged in a rotary drum cooler to lower the temperature to about 60°C by spraying water. The magnetic materials are then transferred to the smelting furnace.

Reduction of the pellets

The furnace is an electric furnace using three Soderberg electrodes. Liquid iron forms the bottom layer whereas a TiO_2 slag is formed on the top. The tapping of liquid iron and titanium slag is done through two different holes. After tapping and cooling, the slag is

crushed to particles finer than 12 mm. The slag is then stored and oxidized for 6 days. The tapped iron is transported in an waggon with an inductive stirring coil. It is then treated at 1575°C, after addition of petroleum coke, ferrosilicon and calcium carbide and hten casted into ingots and water cooled.

Chapter 3

Theory

This chapter provides various knowledge that are necessary to fully understand the purpose and the content of the thesis.

3.1 The Fe-Ti-O ternary system

This part is based on previous studies and works (Taylor et al., 1972; Grey et al., 1974; Jones, 1973; Borowiec and Rosenqvist, 1981).

The understanding of the Fe-Ti-O system is crucial to developp the recovery of the titanium and iron content from ilmenite ores. The knowledge of the phase diagrams is essential because it helps predict the behavior of the ore during oxidation and reduction steps in the industrial process. With this objective, Grey investigated the Fe-Ti-O system by quenching samples previously heated to 1200°C in silica tubes. This way, it is possible to determine which phase is stable at this temperature. In his work, a mapping of the ternary Fe-Ti-O diagram is given at 1200°C. In the area presented below and, four areas are reported.

- The spinel solid solution is limited by magnetite (Fe_3O_4) and ulvöspinel (Fe_2TiO_4) as end points. The point C in the diagram corresponds to a solution of ilmenite in ulvöspinel, assumption made from the excess tetravalent titanium reported. The last end point of the spinel solid solution is point B of composition $Fe_{2.95}O_4$.

- The α-oxide solid solution is limited by the hematite (Fe_2O_3), which is on the Fe-O line. Point F however, is slightly moved towards TiO_2 because this solid solution shows some solubility for rutile (TiO_2). Moreover, this solid solution extends further than the ilmenite composition ($FeTiO_3$) because of the small solubility of Ti_2O_3 in ilmenite. Point G is of composition. $(FeTiO_3)_{0.97}(Ti_2O_3)_{0.03}$

- The next solid solution is the (M_3O_5) solid solution. This solid solution regroups the Fe_2TiO_5 and $FeTi_2O_5$ compounds. The end points of this area are on one side Fe_2TiO_5 and $FeTi_2O_5$ with diluted Ti_3O_5. The global corresponding composition on point J is
$(FeTi_2O_5)_{0.75}(Ti_3O_5)_{0.25}$.

- The last area is not displayed on the diagram and is placed at the K point. This phase is made of a series of reduced rutile which is known as the Magnéli phase series and is obtained at oxygen partial pressures lower than 10^{-14}. In these conditions, pure iron appears to be stable with reduced titanium oxide phase.

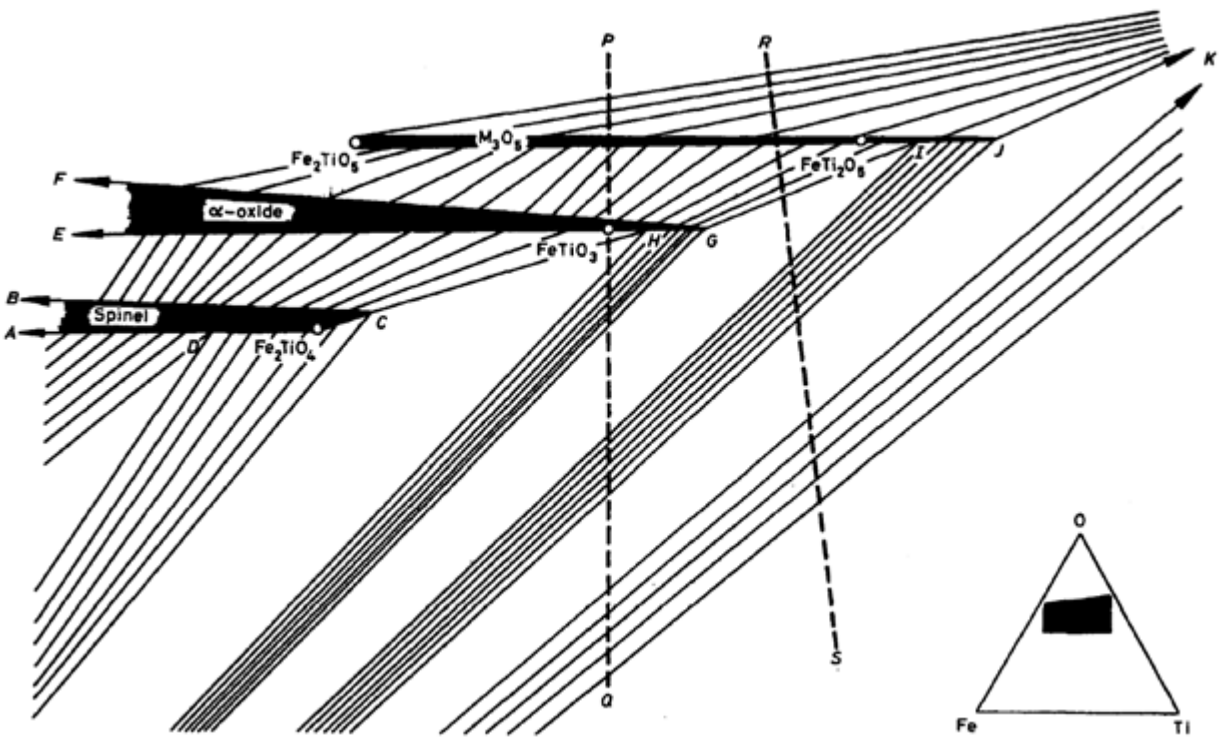

Figure 3.1: Part of the Fe-Ti-O ternary phase diagram at 1200°C representing the three solid solution phases (Grey et al., 1974).

Thanks to Figure 3.1, a first idea of how ilmenite is related to others species is provided.

The possibility of simultaneous existence of these phases has also been reported in the same work.

The stability of these different oxides at high temperature has been reported knowing the free energies of formation (Elliott et al., 1963). In the values presented below in Table 3.1, it is shown that $FeTiO_3$ is stable in a wide range of temperatures. It is then conceivable to obtain ilmenite from the melt with stoichiometric ilmenite composition in an inert atmosphere. We can expect to form an α-oxide solid solution containing mostly ilmenite. However, the composition can slightly deviate from this point in experimental laboratory conditions.

Table 3.1: Free energies of formation of ilmenite (Elliott et al., 1963).

$$Fe_{0.947}(c, l) + 0.053Fe\ (c) + TiO_2(c) \rightarrow FeTiO_3(c, l)$$

T, °K	ΔH°_f cal/mole
298.15	-5800
1200	-4300
1300	-4150
1400	-3950
1500	-3800
1600	-3650
1640 (c)	-3770
1640 (l)	-3770
1650	-3890
1700	-4050
1800	-4800

Assuming a melt containing chemical elements in proportions corresponding to the stoichiometric composition of ilmenite, the result after cooling is to be determined. The lack of information on the cooling only allows assumptions. However, some knowledge has been gathered at fixed temperatures. The question whether or not these states are reached is to be verified experimentally. Moreover, different scenarios might happen due to some small changes of composition with respect to the stoichiometric composition of ilmenite. These situations have to be taken into account given that experimental conditions are likely to deviate from ideality. The three next scenarios are built according to the Figure 3.2 which gives a overview of the Fe-Fe_2O_3-TiO_2 system, and that the product is obtained from a melt.

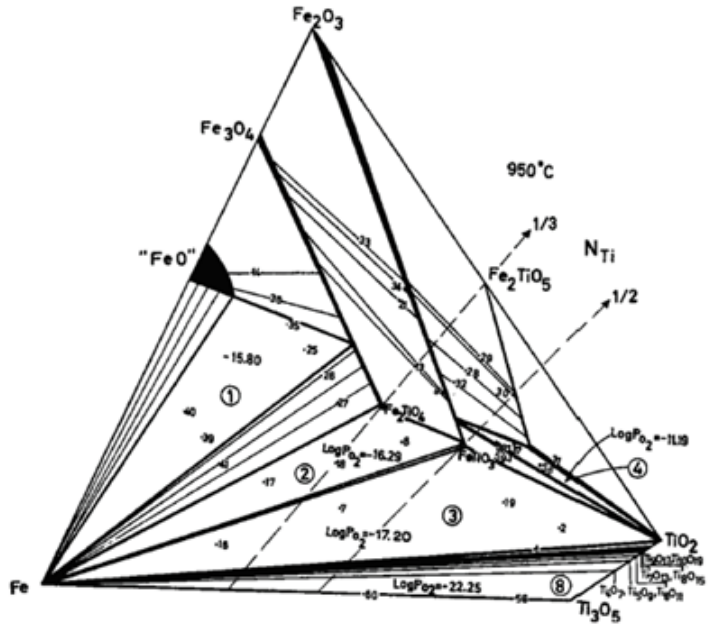

Figure 3.2: Fe-Fe_2O_3-TiO_2-Ti_3O_5 phase diagram at 950°C (Borowiec and Rosenqvist, 1981)

Assumption 1: Excess iron in the melt

Assuming excess iron in the melt from Fe_2O_3, TiO_2 and Fe, it appears that the composition is placed on the Fe-$FeTiO_3$ line. In this area, a mix of ilmenite and iron is obtained. As seen before, the solubility of pure iron in ilmenite is not extensive in the α-solid solution at 1200°C. It is then expected that most of excess iron is expelled from ilmenite during cooling, since the solidification of iron happens before the one of ilmenite. Because of iron density, some iron is expected on the bottom of the product after cooling of the melt.

Assumption 2: Lack of titanium oxide TiO_2

In the case of a lack of titanium oxide, the composition of the melt would be placed somewhere on the Fe_2TiO_4 and $FeTiO_3$ line. This diagram then shows that ulvöspinel (Fe_2TiO_4) is found with such melts. In this situation, Fe_2TiO_4 and $FeTiO_3$ are expected to form two dinstinct phases given that ülvospinel, here the minor component, is not soluble in ilmenite.

Assumption 3: Lack of iron (III) oxide(Fe_2O_3)

Such a composition, according to the diagram is located in the third area, corresponding to a mix of iron metal, titanium oxide and ilmenite. As a result, in case of a lack of iron oxides, Fe_2O_3, some iron metal and titanium oxide will be formed in adition to ilmenite during the cooling. In this situation the melt would then contain excess titanium oxide and iron relative to the ilmenite composition. The diagram at 1200°C in Figure 3.1 shows that ilmenite's solid solution extends further than $FeTiO_3$, away from Fe_2O_3. This shows a solubility of titanium oxide in ilmenite. It is then possible to consider the existence of titanium oxide expelled from ilmenite late in the cooling process. This titanium oxide would then be found mixed in the solidified product. The existence of an iron precipitate in solidified ilmenite remains to be proven.

3.2 The Fe-Mg-Ti-O quaternary system

This system has been extensively studied in the temperature range 900-1100°C (Borowiec and Rosenqvist, 1985). Borowiec's work as been used to prepare this section.

The next diagrams in Figure 3.3 show the ternary system MgO-TiO_2-FeO that is useful for this study. In order to investigate the impact of Mg in ilmenite, the synthesis of Mg-rich ilmenite is of interest. The objective is then to find a way to synthesize the $FeTiO_3$-$MgTiO_3$ solid solution (M_2O_3 solid solutions). Another challenge is to avoid the $FeTi_2O_5$-$MgTi_2O_5$ solid solution (M_3O_5 solid solution). The question is then to determine whether or not it is possible to produce such a composition in laboratory conditions.

As displayed in the diagrams, a three phase area is present in the low-right corner at 1100°C. This area corresponds to a mix of TiO_2, M_3O_5 solid solution and the M_2O_3 solid solution. This means that in order to synthesize a product containing $FeTiO_3$ and $MgTiO_3$ and without pseudobrookite ($FeTi_2O_5$), this area must be avoided.

The diagram at 900°C, however, shows that this three phase area is shifted towards $MgTi_2O_5$ with decreasing temperature. This means that a slow cooling could help achieve the aim of avoiding a $FeTi_2O_5$-$MgTi_2O_5$-TiO_2 system while keeping the $FeTiO_3$, $MgTiO_3$ and TiO_2 compounds. Since the titanium oxide is not considered as a problematic compound in the final product, it is interesting as well to add a little amount of TiO_2 in excess prior melting. This also ensures that in case of an incomplete melting of the ox-

ides, the TiO_2 content is still high enough to obtain the composition on the right side of the $FeTiO_3$-$MgTiO_3$ curve.

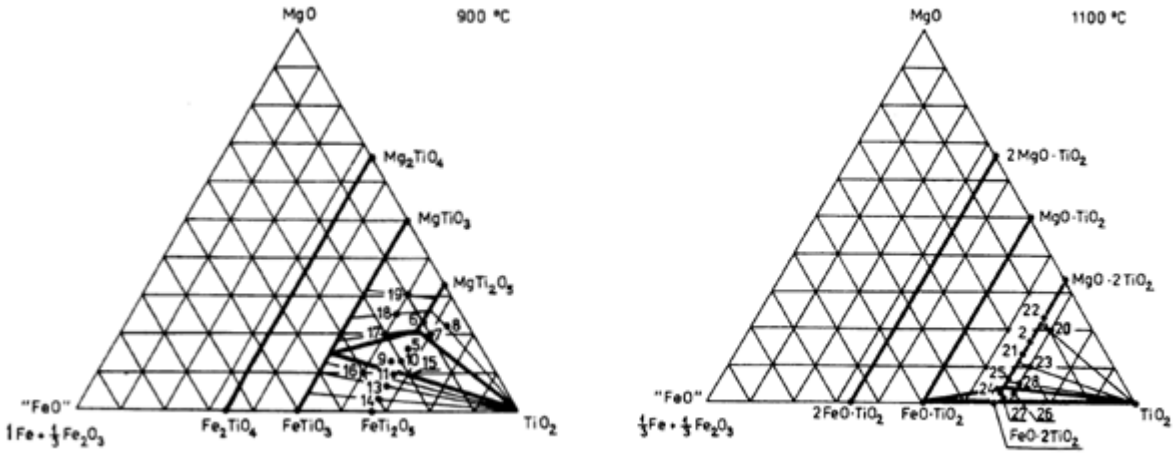

Figure 3.3: Pictures of the MgO-TiO_2-FeO ternary phase diagrams at 900°C and 1100°C (Borowiec and Rosenqvist, 1985)

3.3 Critera for the crucible

One of the technological problems for ilmenite synthesis through melting consists in finding the proper furnace to use. In his paper, Pistorius states that ilmenite smelting requires a special crucible due to the corrosivity of high titania slag (Pistorius, 2003). The technical solution is to use a freeze lining that prevents the damage to the crucible, by protecting it with a frozen layer of the molten materials. Given that the system studied, Fe-Ti-O, leads to a similar chemical composition, using traditional refractories is impossible. Previous work has used a water cooled copper crucible successfully. Seim managed to investigate the $FeTiO_3$-Ti_2O_3-TiO_2 Slag System (Seim, 2011). The species being the same, this copper crucible is an appropriate solution to the corrosivity problem.

3.4 Pre-oxidation of pellets

As mentioned in a previous study, pre-oxidizing the ilmenite is considered to improve the following reduction (Lobo et al.). Vijay states that the reducibility is improved and the reduction temperature is decreased due to the pre-oxidation (Vijay et al., 1996). Hussein suggested that the pre-oxidation, which reached 75 to 80 percent of the maximum

oxidation, might be limited by the forming of a solid-solution resisting further oxidation (Hussein et al., 1967). Jones describes the oxidation of ilmenite at temperatures higher than 800°C by the following Equations 3.1, 3.2 (Jones, 1973). He also notes that the reaction is incomplete at 1000°C.

$$2FeTiO_3 + \frac{1}{2}O_2 = Fe_2TiO_5 + TiO_2 \tag{3.1}$$

$$Fe_2Ti_3O_9 = Fe_2TiO_5 + 2TiO_2 \tag{3.2}$$

Gupta confirms the pseudorutile ($Fe_2Ti_3O_9$) decomposition at 700°C to 1000°C in both air and oxygen (Gupta et al., 1991). According to his study, pseudorutile is also formed as an intermediate product. The mechanisms he proposes are shown in Figure 3.4:

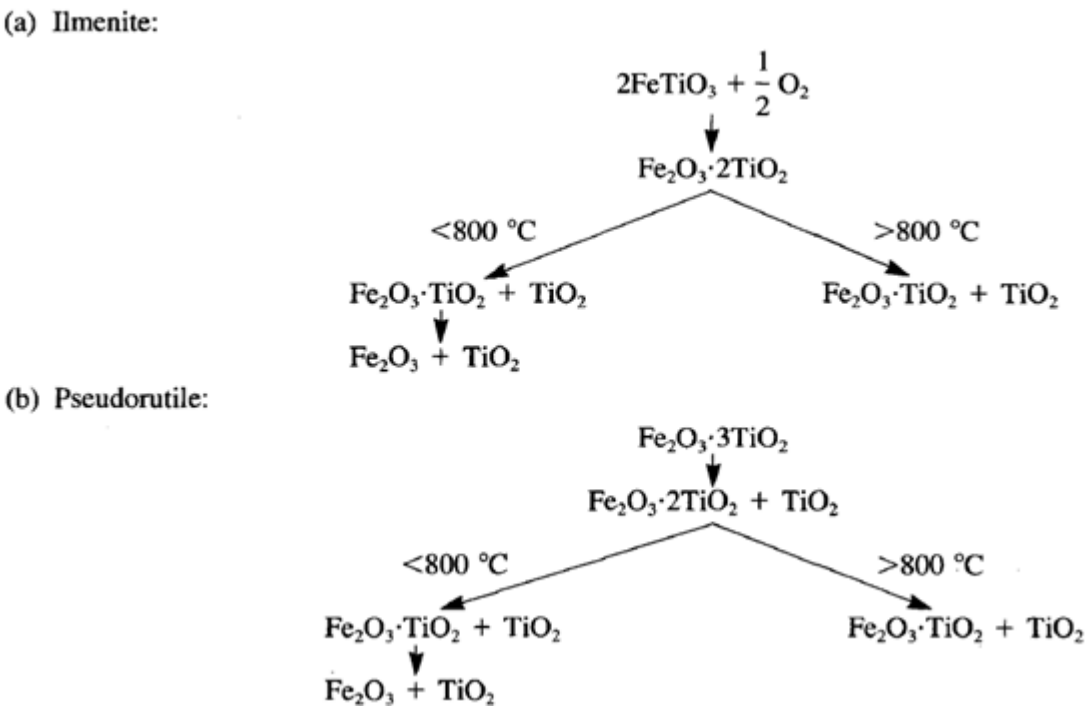

Figure 3.4: Oxidation paths of ilmenite and pseudorutile (Gupta et al., 1991).

In this figure, Gupta shows that pseudorutile leads to the production of a $Fe_2O_3{\cdot}2TiO_2$ intermediate product. The products of the global reactions remain the same. At temperatures higher than 800°C, $Fe_2O_3{\cdot}2TiO_2$ formed from ilmenite decomposes according to Equation 3.3:

$$Fe_2O_3 \cdot 2TiO_2 = Fe_2O_3 \cdot TiO_2 + TiO_2 \tag{3.3}$$

The pre-oxidation is in the end producing pseudobrookite (Fe_2TiO_5) and rutile (TiO_2) at temperatures higher than 800°C, but leads to hematite (Fe_2O_3) and rutile (TiO_2) at temperatures below.

3.5 Reduction of pellets

Many papers report the mechanisms of gaseous reduction of pseudobrookite Fe_2TiO_5 by CO gas and H_2 gas. Jones explains that the reduction reaction holds in two steps: the reduction from iron (III) to iron (II) state (Equation 3.4) followed by the reduction from iron (II) to iron metal (Equation 3.5). These mechanisms are described by the following equations (Jones, 1973; Sun et al., 1992) with either CO or H_2 as reductant (R):

$$Fe_2TiO_5 + TiO_2 + R = 2FeTiO_3 + RO \tag{3.4}$$

This equation is applicable when the sample is brought to temperature under inert atmosphere.

$$FeTiO_3 + R = Fe + TiO_2 + RO \tag{3.5}$$

The reaction of potential hematite left in the reactants with CO and TiO_2 at 900°C is also given by Jones, and described as follow:

$$Fe_2O_3 + 2TiO_2 + CO = 2FeTiO_3 + CO_2 \tag{3.6}$$

Further reactions of titanium oxide reduction leading to reduced rutile phases as also been reported (Lobo et al.).

To summarize, the reduction reaction is divided into two different steps, the reduction of pseudobrookite into ilmenite followed by the reduction of ilmenite into the final products. These reactions can be followed by a further reduction of rutile into reduced rutile.

3.6 Fluid particle reactions

This part has been prepared using the chapter 25 of the book Chemical Reaction Engineering (Levenspiel, 1999). The points presented below are key elements to the comprehension of Gas-Solid reactions.

Reaction type and Model

Among the various kinds of gas-solid reactions, the type useful for this study is the following:

$$A(fluid) + bB(Solid) \rightarrow \text{fluid and solid products} \tag{3.7}$$

In reactions such as those of this study, the reduction of metals from their oxides, the solid doesn't change in size in a significative way. The particles are not reducing in size during the experiment although they react. Different models exist to explain the mechanisms.

- The PCM, or Progressive-Conversion Model, corresponds to the case when the reactant can enter everywhere in the particle all the time. In this situation, the conversion is continuous and happens in all the particle. A representation of such a mechanisms is given in Figure 3.5.

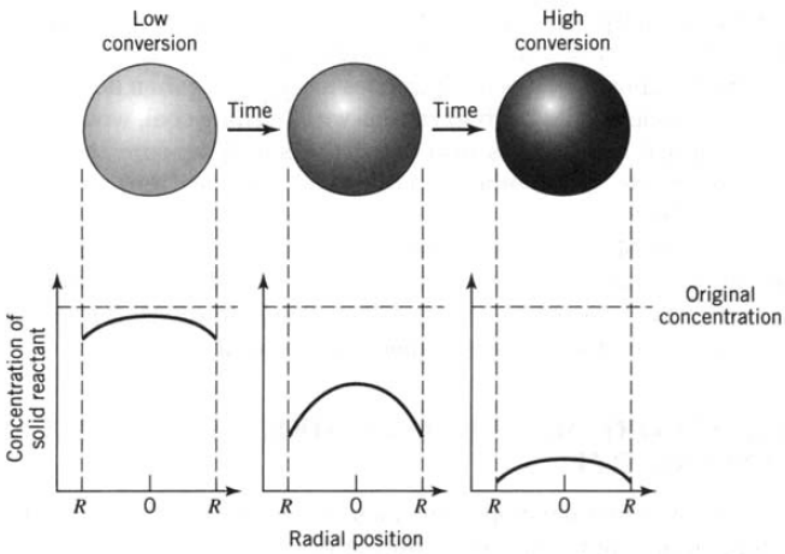

Figure 3.5: Reaction of a particle acccording to the PCM Model (Levenspiel, 1999).

- The SCM, or Shrinking-Core Model, corresponds to the case when the reactant only acts on the edge of the particle, before reacting deeper. As a result, an unreacted core remains in the center of the particle but is reducing in size as the reaction progresses. This model has shown to represent better the reality in most of the situations. An overview of this mechanism with time is shown is Figure 3.6.

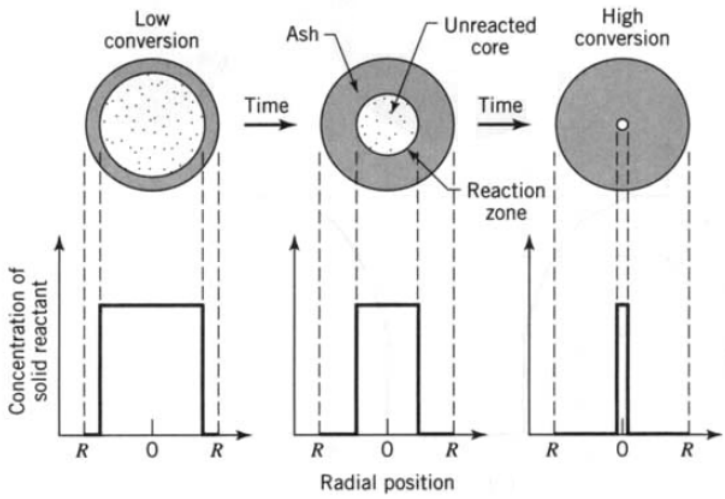

Figure 3.6: Reaction of a particle acccording to the SCM Model (Levenspiel, 1999).

The shrinking core model

Five steps have been reported by Yagi and Kunii to occur during the reaction (Levenspiel, 1999).

1. The gaseous reactant diffuses to the surface of the particle from the bulk gas.
2. The gaseous reactant goes through the already reacted layer (ash/product layer) and penetrates the unreacted core.
3. The gas-solid reaction occurs.
4. The gaseous product goes through the already reacted layer.
5. The gaseous product diffuses to the bulk gas.

For spherical particles, three possible steps could possibly be rate limiting, or even a combination of these steps. In the following paragraphs, the equations behind the mechanisms are detailed. The stoichiometry used in Equation 3.7 is to be noted.

Diffusion through the gas film as limiting step

In Figure 3.7 a representation of the reaction mechanisms when the limiting step is the gas diffusion is given. The reactant A decreases in concentration close to the particle. The diffusion being too slow, the reaction exhausts the content of available reactant A close to the surface. The new available A is then supplied by diffusion mechanisms at a constant pace since both the bulk concentration and the surface concentration are kept constant. Because of the stoichiometry in Equation 3.7, $dN_B = bdN_A$, Levenspiel gives:

$$-\frac{1}{S_{ex}} = -\frac{1}{4\pi R^2}\frac{dN_B}{dt} = -\frac{b}{4\pi R^2}\frac{dN_A}{dt} = bk_g(C_{Ag} - C_{As}) = bk_g C_{Ag} = constant \tag{3.8}$$

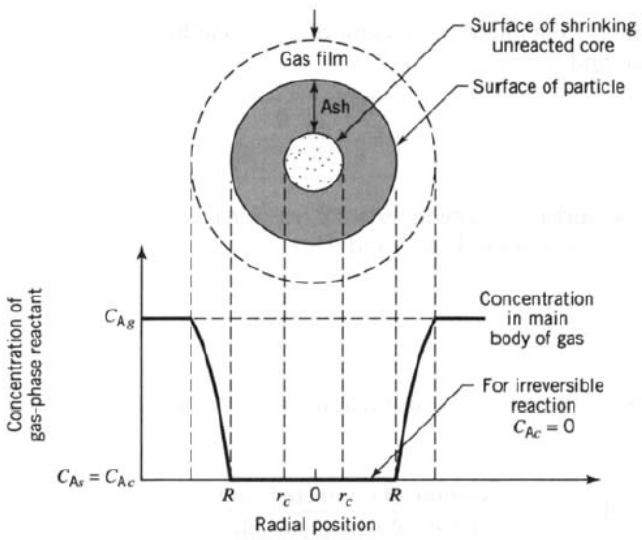

Figure 3.7: Representation of a particle during the reaction when the gas diffusion is the limiting step (Levenspiel, 1999).

By replacing the amount of B by its molar density times the volume of solid reactant left at a time, the equation becomes:

$$-\frac{1}{S_{ex}} = -\frac{\rho_B r_c^2}{R^2}\frac{dr_c}{dt} = bk_g C_{Ag} \tag{3.9}$$

By integrating, the time needed to reach a certain depth is obtained. The time for full reaction (τ) is given with $r_c = 0$.

$$t = \frac{\rho_B R}{3bk_g C_{Ag}}\left[1 - \left(\frac{r_c}{R}\right)^3\right] = bk_g C_{Ag} \tag{3.10}$$

$$\tau = \frac{\rho_B R}{3bk_g C_{Ag}} \tag{3.11}$$

Therefore,

$$\frac{t}{\tau} = 1 - \left(\frac{r_c}{R}\right)^3 \tag{3.12}$$

Diffusion through the ash layer as limiting step

In Figure 3.8, the case of an ash layer diffusion as limiting step is shown. Levenspiel explains the mechanisms with an analysis in two steps. Because the shrinking of the core is much slower than the diffusion of the particles, it is possible to consider it stationary. The reaction is then controlled by the rate of diffusion of A, i.e.

$$-\frac{dN_A}{dt} = 4\pi r^2 \mathcal{Q}_A = 4\pi r^2 \mathcal{Q}_{As} = 4\pi r^2 \mathcal{Q}_{Ac} = constant \tag{3.13}$$

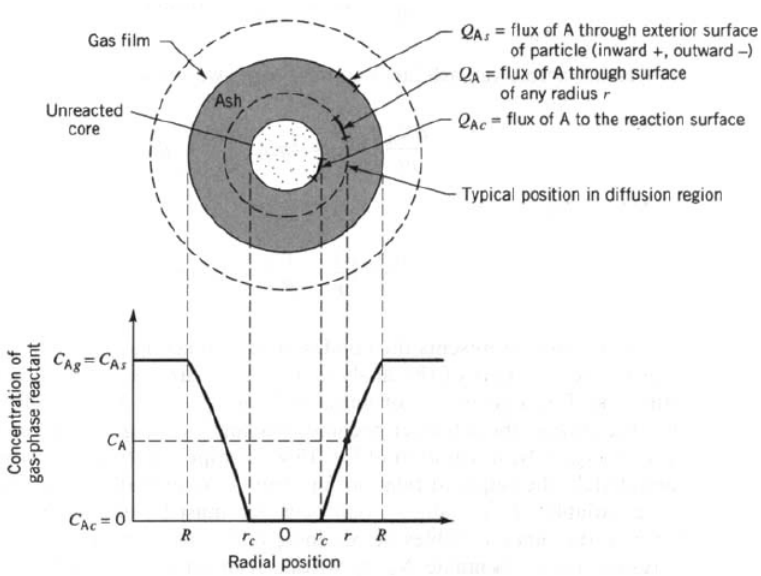

Figure 3.8: Representation of a particle during the reaction when the diffusion through the ash layer is the limiting step (Levenspiel, 1999).

By using the effective diffusion coefficient the next equation is obtained:

$$-\frac{dN_A}{dt} = 4\pi r^2 \mathcal{D}_e \frac{dC_A}{dr} = constant \tag{3.14}$$

After integration, Equation 3.14 becomes:

$$-\frac{dN_A}{dt}\left(\frac{1}{r_c}-\frac{1}{R}\right)=4\pi r^2\mathscr{D}_e C_{Ag} \tag{3.15}$$

At this point, the change of size of the core is to take into account. Since the problem contains three variables t, N_A and r_c, one has to be eliminated to integrate. N_A can be written as a function of r_c, as done before in Equation 3.9. After integration, the relationship between time and radius of the core is:

$$t=\frac{\rho_B R^2}{6b\mathscr{D}_e C_{Ag}}\left[1-3\left(\frac{r_c}{R}\right)^2+2\left(\frac{r_c}{R}\right)^3\right] \tag{3.16}$$

For complete conversion and fractional conversion, the results are the following:

$$\tau=\frac{\rho_B R^2}{6b\mathscr{D}_e C_{Ag}} \tag{3.17}$$

$$\frac{t}{\tau}=1-3\left(\frac{r_c}{R}\right)^2+2\left(\frac{r_c}{R}\right)^3 \tag{3.18}$$

Chemical reaction as limiting step

As the last case to consider, Levenspiel explains the chemical reaction. The reaction is only affected by the surface of the unreacted core, and not by the ash layer. A representation of a particle during reaction when the chemical step is the limiting one is given in Figure 3.9. With k" as the first order rate constant for the reaction, the equation is:

$$-\frac{1}{4\pi r_c^2}\frac{dN_B}{dt}=-\frac{b}{4\pi r_c^2}\frac{dN_A}{dt}=bk''C_{Ag} \tag{3.19}$$

After replacing N_B by the density times the volume in terms of r_c, and after integration, the relation between the time and the radius is:

$$t=\frac{\rho_B}{bk''C_{Ag}}(R-r_c) \tag{3.20}$$

The time at complete reaction and fractional conversion are then:

$$\tau=\frac{\rho_B R}{bk''C_{Ag}} \tag{3.21}$$

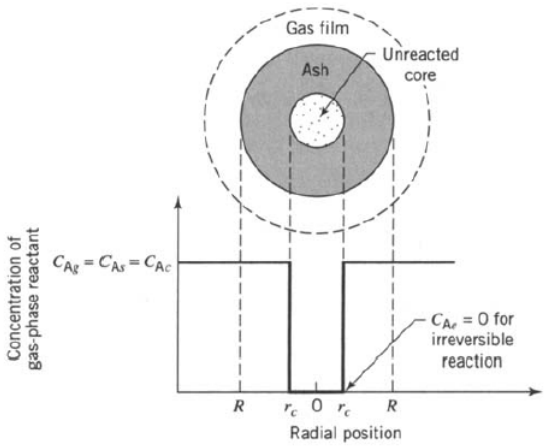

Figure 3.9: Representation of a particle during the reaction when the chemical reaction is the limiting step (Levenspiel, 1999).

$$\frac{t}{\tau} = 1 - \frac{r_c}{R} \tag{3.22}$$

Extensions and limitations

Although each of the steps has been seen before as the limiting one, the reality might not fit any of these situations. Indeed, the different steps are acting simultaneously. The use of the total time as a combination of the different steps gives a better picture of the reality. Thus:

$$\tau_{\text{total}} = \tau_{\text{film alone}} + \tau_{\text{ash alone}} + \tau_{\text{reaction alone}} \tag{3.23}$$

According to Levenspiel, however, the shrinking core model can not answer explain alone the reality. One of the exception given in his book, the slow reaction of a very porous solid, is of interest. According to him, in such a situation, the continuous reaction model might be a better model to explain the mechanisms. However, no precisions on the porosity nor the reaction speed was specifically given.

Determine the rate limiting step

To know what the rate limiting step at a time is, some parameters can be modified. These parameters are few suggestions on what to vary to distinguish the limiting steps, and are given by the author as a guide for experiments.

- Temperature: Since the temperature is generally more impactful on the chemical reaction, varying the temperature of reaction might help to investigate is the chemical reaction is the limiting step.

- Particle Size: the different mechanisms proposed have a different dependance on the dimensions of the particle. For example, in a chemical reaction, the dependance will be such that $t \propto R$. If the limiting step is the ash diffusion, $t \propto R^2$. Having runs with different particle size is then of interest to investigate the impact of the particle size.

- Gas flow: To distinguish between gas film and ash layer as limiting step, varying the gas velocity is to be considered. The diffusion in the ash layer is indeed not influenced by the bulk gas speed.

Chapter 4

Experimental

The reduction experiments have been carried on ilmenite pellets made in laboratory. This section presents the various experimental steps, from the material synthesis to the characterization methods.

4.1 Materials

Ilmenite was prepared by melting of a mix of high purity powders and pieces of Fe_2O_3, Fe and TiO_2. The different materials chosen are:

- Iron pieces, irregularly shaped, 3.2-6.4mm, 99.99% purity (metals basis)
- TiO_2 evaporation pieces, 1-4mm, 99.95% purity
- Iron (III) oxide Fe_2O_3, ≤ 5µm, ≥99% purity

4.2 Synthesis in the cold crucible induction furnace

Two batches were prepared in order to produce enough quantities of raw material for pelletizing. The production process involved results from the previous work of the author (Canaguier, 2013b) but with slightly different parameters. During this earlier project, the behavior of the furnace had been investigated, in order to acquire its functioning principles. At this time, 5 experiments of synthesis from pure compounds were carried out. These attempts showed that reaching temperatures up to 1700°C helps to obtain a fully reacted batch. This led to a better choice of power input for this work.

In this study, the components have been mixed to form stoichiometric ilmenite. The material weight corresponding to the two batches is reported in Table 4.1 .

The equipment used for melting of the powders is a cold crucible induction furnace. This setup is made of a power supply from Farfield Electronics PTY Ltd and a water cooled copper crucible from ANSTO and is showed in Figure 4.1. This setup has been used previously for ilmenite slag production (Seim, 2011) but was also used for ilmenite synthesis by the author in an earlier work (Canaguier, 2013b).

A boron-nitride coating was used on the walls of the crucible. The iron and titanium oxides mix was inserted in the bottom of the crucible and packed manually. The pure iron pieces were placed concentrated on the top to optimize the induction effect. Once insulated, the crucible has been evacuated with a rotary pump to remove the remaining air, and then filled with argon at atmospheric pressure. The argon flow was maintained during the experiments at a flow of 1L/min.

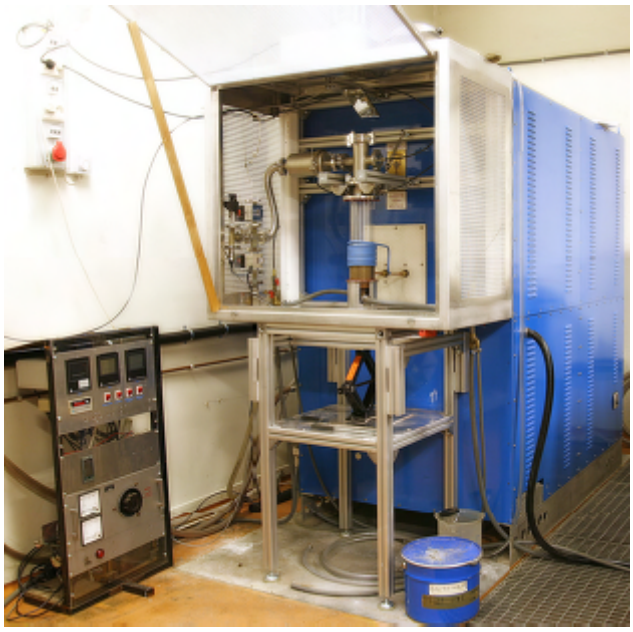

Figure 4.1: Picture of the cold crucible induction furnace.

The melting was carried under argon atmosphere at atmospheric pressure and to temperatures reaching 1600°C. The current intensity used corresponds to 70% of the maximum current available with the furnace. The holding time, time between the increase and the decrease of the current, was 8 min for both batches. The rapid cooling was done by stopping the heating, i.e. the current, while keeping the water cooling on the crucible. The product was then manually removed from the crucible.

Table 4.1: Sample parameters for ilmenite synthesis

Sample parameters	Charge Fe_2O_3 [g]	Charge TiO_2 [g]	Charge Fe [g]	Charge MgO [g]	Total mass [g]	Holding time [min]	Run order
Ilmenite Synth. Batch 1	105.26	157.95	36.8	0	300.01	8	1
Ilmenite Synth. Batch 2	105.3	157.95	36.85	0	300.1	8	2
Mg-rich ilmenite	93.2	162.0	32.6	3.7	291.5	8	3

Mg-rich ilmenite synthesis

Few parameters were changed for this particular experiment although most of the features are the same. Here the differences between pure ilmenite and Mg-rich ilmenite synthesis are explained. First, approximatively 30% of the Fe_2O_3-TiO_2 mix was placed in the crucible, before placing the MgO powder. A total of 5% of MgO in terms of mass was added to the reactants. The rest of the Fe_2O_3-TiO_2 mix was then added on the MgO layer. As explained for the ilmenite synthesis, iron was placed concentrated on the top. However, a small layer of iron pieces was also placed on the oxide materials to prevent crust forming. Because of the findings on the ternary diagram of the MgO-TiO_2-FeO system, modifications were done on the cooling path. In order to reach temperature below 900°C, the power supply initially set at 70% was decreased by 5% every two minutes.

4.3 Pelletizing

The crushed synthesized ilmenite powders from two different batches were mixed together with 0.8% bentonite. The mixing was done in a TURBULA mixer of type T2C for one hour. Once properly mixed, the powder has been used to produce pellets in a pelletizing drum shown in Figure 4.2.

First, small seeds have been produced to start the pelletizing at an inital speed of 70 rpm. The speed of the drum has been lowered during the pelletizing while material and water were added progressively and pellets growing. Given the small quantity of material available for pelletizing, some undersized pellets have been dried and crushed to be reintroduced as raw materials in the pellet drum. The product has later been screened to obtain pellets around 10 mm. In the end, 241.5g of +9 mm/-10mm and 242.75 of +10 mm of green pellets were produced. The obtained mass after drying was 212.02g of +9mm/-10mm and 204.06g of +10mm. The pelletizing was done by both Edith Thomassen from SINTEF and the author.

4.4 Pre-oxidation

The two different pellet sizes previously obtained were oxidized together in the same run, but in different crucibles. Alumina crucibles were used as containers. The furnace used is a

Figure 4.2: Picture of the pelletizing drum.

muffle furnace of type Nabertherm N17 /HR Controller C290. In order to avoid potential cracks in the pellets due to moisture, the pellets were introduced at the beginning of the temperature increase in the oven. The temperature increase lasted two hours until 1000°C. The holding time was 2h before the pellets were removed from the furnace and cooled in air. Real time measurements have been done using a thermocouple positioned between the two crucibles.

4.5 Gaseous reduction

Two experiments were carried out in a TGA vertical retort furnace, in order to investigate the gaseous reduction of the lab-made ilmenite pellets. After the sintering, the two obtained batches were mixed in a steel pan to have a similar pellet size distribution in both experiments. Two different batches were prepared according to Table 4.2.

The set-up consists of a suspended crucible through wires connected to a balance. This crucible is also connected to two gas tubes free of movement in order to limit their impact on the weight measurement. The Figure 4.3 shows the set-up and its compounds.

The thermocouple sheath is placed in the middle of the crucible. The pellets are placed

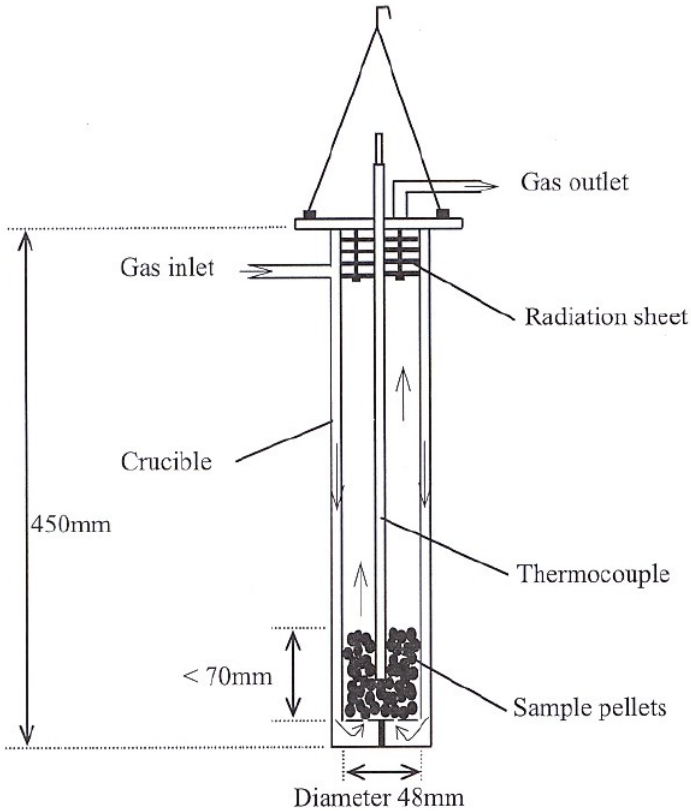

Figure 4.3: TGA Crucible (Sunde, 2012).

in a container with dimensions similar to those of the crucible, to know the height of the sample load. The materials are then loaded in the crucible, and the top part is sealed using a graphite gasket. The sheath is raised of approximately half of the height measured earlier to ensure an accurate temperature measurement.

Once prepared, the crucible is attached to the balance, a Mettler Toledo model PR2003DR. The crucible is hanging in the middle of an Entech resistance furnace model VTF 801/12, where all physical contact is avoided between the crucible and the furnace. The gas flow is controlled by Bronkhorst model F201c mass controllers.

In both experiments carried out with the TGA furnace, the furnace temperature was set to 958°C. This is done because previous experiments showed the difference between furnace set point and crucible temperature. The warm up lasted 1h45min under an argon flow of 1L/min. The argon flow was then increased to 5L/min to ensure a constant gas flow when changing to the reduction gas (CO or H_2 at atmospheric pressure). The reduction conditions are then maintained for 4h. After the reduction, the gas flow is shifted back to 1L/min of argon and the heating stopped. Note that the different steps of the experiment

only change one parameter (gas flow, gas composition, temperature...) at a time. This is done to reduce uncertainty. A sum-up of the main parameters used for the experiments carried out is provided below in Table 4.3. During the experiment, mass loss measuerment were carried out.

The conversion degree is obtained from the mass loss measurements. The formula for the conversion degree calculation is given in Equation 4.1 by assuming all the iron is in trivalent form before reduction.

$$\text{Conversion degree} = \frac{\Delta m}{m \cdot \%O \cdot \frac{3}{7}} \tag{4.1}$$

With m the initial mass of the sample, Δm the mass change and %O the weight percentage of oxygen in the sample.

Table 4.2: Size distribution of the ilmenite pellets in the different batches

	+9/-10mm pellets [g]	+10mm pellets [g]	Total mass [g]
Batch CO experiment	105.62	101.24	206.76
Batch H2 Experiment	106.18	102.41	208.59

Table 4.3: Experiment parameters for the gaseous reduction.

Sample Name	Oxidation temperature (°C)	Mass before reduction (g)	Gas flow rate	Time	Furnace set-point (°C)	Average temperature (°C)	Gas
10.10-C-synth.ilm	1000	206.76	5 L/min	4hr	958	995.2	CO gas
10.10-H-synth.ilm	1000	208.59	5 L/min	4hr	958	996.2	H_2 gas

4.6 X-ray diffraction

The X-Ray Diffraction measurements were carried at NTNU at the Institute of Material Technology. The powders were placed in sample holders. The instrument used is a D8 DaVinci diffractometer, and each of the samples has been analyzed for 15 minutes. This duration is long enough to have a sufficient signal/noise ratio. The incident angle band used is 5° - 60°, and the V6 parameter was enabled. After analyzing, the software Diffrac.Eva was used to match the X-ray diffraction graphs. To determine the different species present most references used were star (*) ones, from the PDF -4+ 2013 RDB database, which are of better quality overall.

4.7 Electron probe micro-analysis

Two samples corresponding to the two different gas reduction experiments have been prepared for an electron probe micro-analysis. The samples have been mounted in epoxy and then polished before being carbon coated prior the analysis. The equipment used is a JEOL JXA-8500F. Pictures were taken on three different depths in the pellet: close to the surface, at 2mm deep, and at 4mm deep. Moreover, for each of these positions, the pictures were done at three different magnifications: 500x 1000x and 2000x. Mapping, secondary imaging as well as quantitative point analyses on many phases has been done. The quantitative point analysis was done in the areas pictured at maximum magnification, and three point analysis were done per apparent phase.

Chapter 5

Results

The results are presented in this chapter. First, results concerning the synthesis of ilmenite and Mg-rich ilmenite are shown, followed by the various results from intermediary steps before reduction. Finally, results of the reduction are presented with multiple methods.

5.1 Synthetic ilmenite

The two different batches produced led to different results. Visually, the same phenomenon has been reported: a crust is remaining on the top containing partly reacted material of TiO_2 and Fe_2O_3. This crust was covering part of the product so that approximately one third of the section was covered. This has been observed in both batches, but with different configuration. A slightly different quantity of crust was formed in the two experiments.

The product itself was completely reacted in the bottom part of the crucible, and was visually homogeneous. After breaking, the inside also looked homogeneous, but trapped an iron ball at the bottom of the product.

Some of the boron-nitride coating was fixed to the product on the edges in negligible quantities, and was removed after washing by hand.

Mg-rich synthetic ilmenite

The Mg-rich ilmenite synthesis showed some differences with the pure ilmenite synthesis. First, no crust has been observed during this experiment. However, some splashing occured, ejecting materials on the protecting glass. An iron piece was also found in the bottom of the product. Visually, the product also looked more porous than for pure

ilmenite synthesis but the shape, shown in Figure 5.1, looked similar overall .

Figure 5.1: Picture of the product after removal from the crucible.

5.2 Synthetic ilmenite powder

Particle sizing

After crushing, the black powder obtained has been analyzed for particle size. Figure 5.2 and 5.3 show the results of this analysis for the pure ilmenite synthesis. From these analyses, which are very similar for the two different batches, it comes that about 80% of the volume made of particles between approximately 10-300 µm. The peak of volume frequency is around 150 µm in both samples. We can also notice that some particles size is up to 500 µm.

Ilmenite composition

In Figure 5.4 and 5.5, the XRD results for the synthetic product are shown. In the first batch, ilmenite of reference PDF 01-073-1255 has been detected has the dominant phase. However, other species are also evidenced such as pure iron (Fe) of reference PDF 00-006-0696, and titanium oxide (TiO_2) of reference PDF 00-003-1122. These second peaks are rather limited in size. The ilmenite peaks are represented in red and spotted by a "Ilm". The rutile peaks are in green and spotted by a "R". Finally, the iron peak is in blue and spotted by a "Fe"

The second batch shows again a strong dominance of the ilmenite phase, but different impurities. Indeed, this time, ülvospinel (Fe_2TiO_4) of reference PDF 04-016-9481 is de-

tected by the XRD. The ilmenite phase detected in the second sample is of same reference as in the first one. Again, the secondary set of peaks, corresponding to ülvospinel, are limited in size. This means that the quantity of ülvospinel is rather limited compared with the quantity of ilmenite. On the graph, the ilmenite peaks are represented in red and spotted with a ”Ilm”. The ülvospinel peaks are in blue and spotted by a ”U”.

These two graphs show that ilmenite is the most important phase in these samples, with a few of well-known impurities. However no quantitative analyses is given through these XRD analyses.

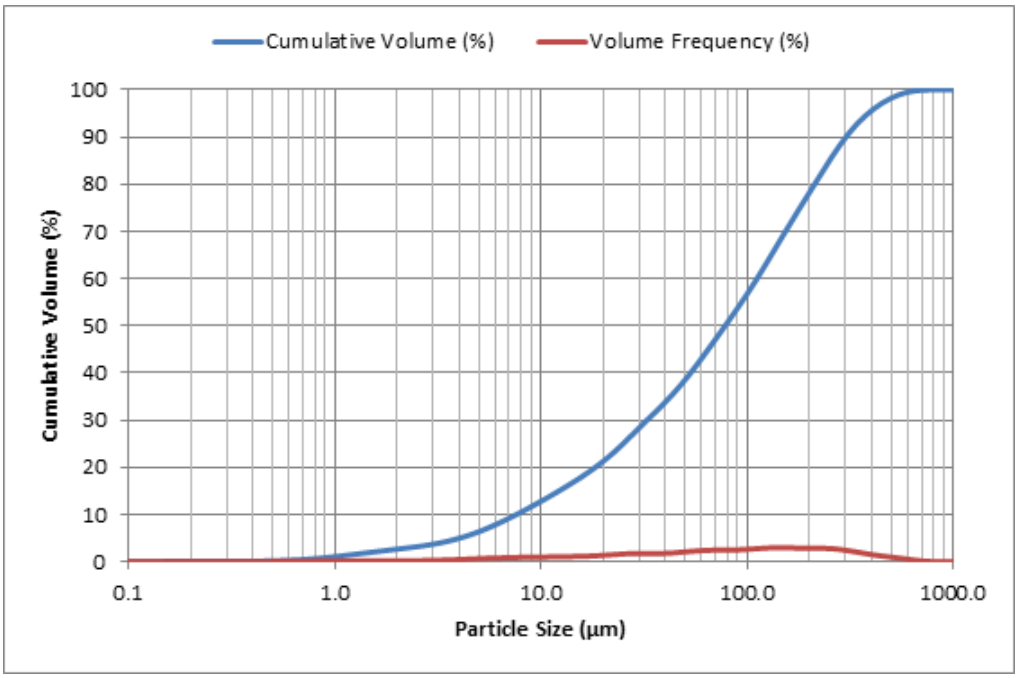

Figure 5.2: Particle sizing for synthetic ilmenite batch 1.

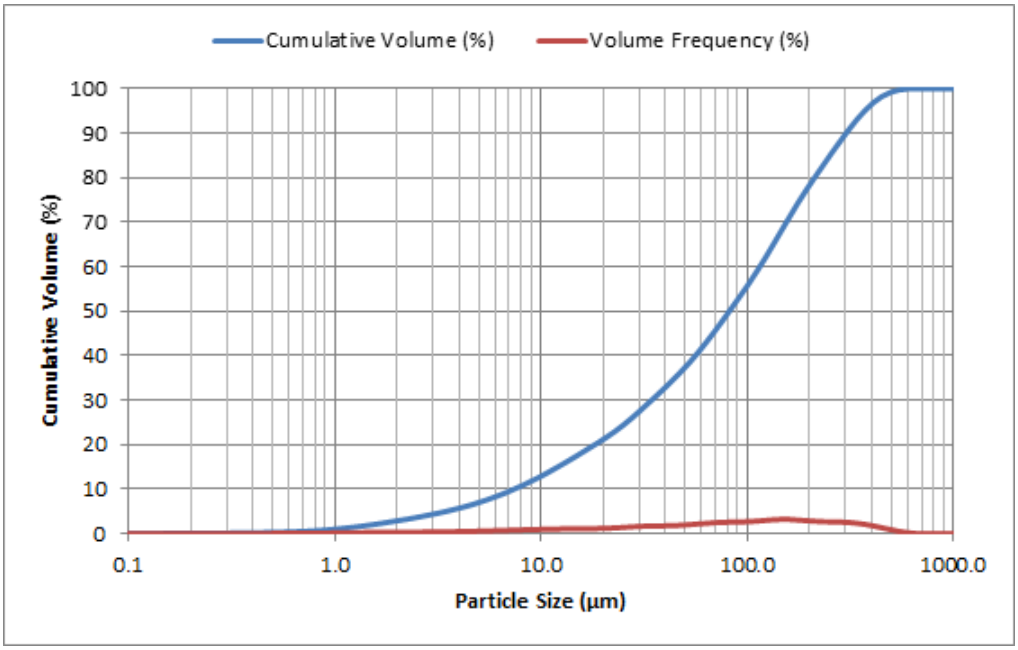

Figure 5.3: Particle sizing for synthetic ilmenite batch 2.

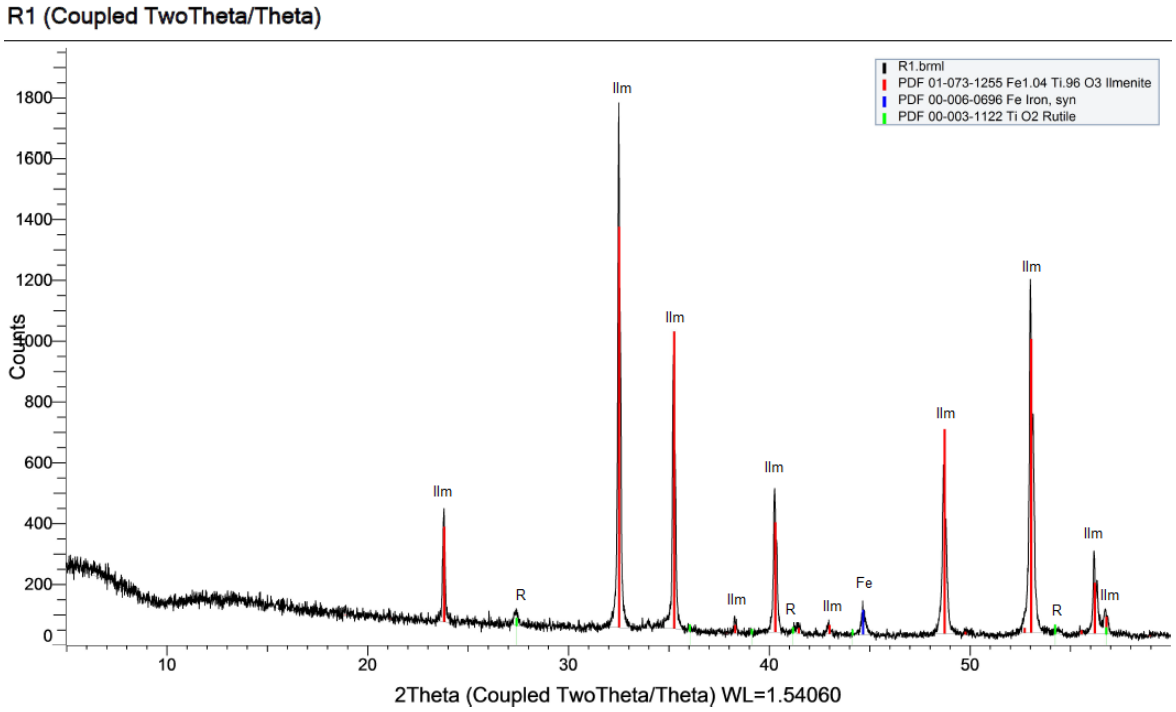

Figure 5.4: X-Ray Diffraction analysis for synthetic ilmenite batch 1.

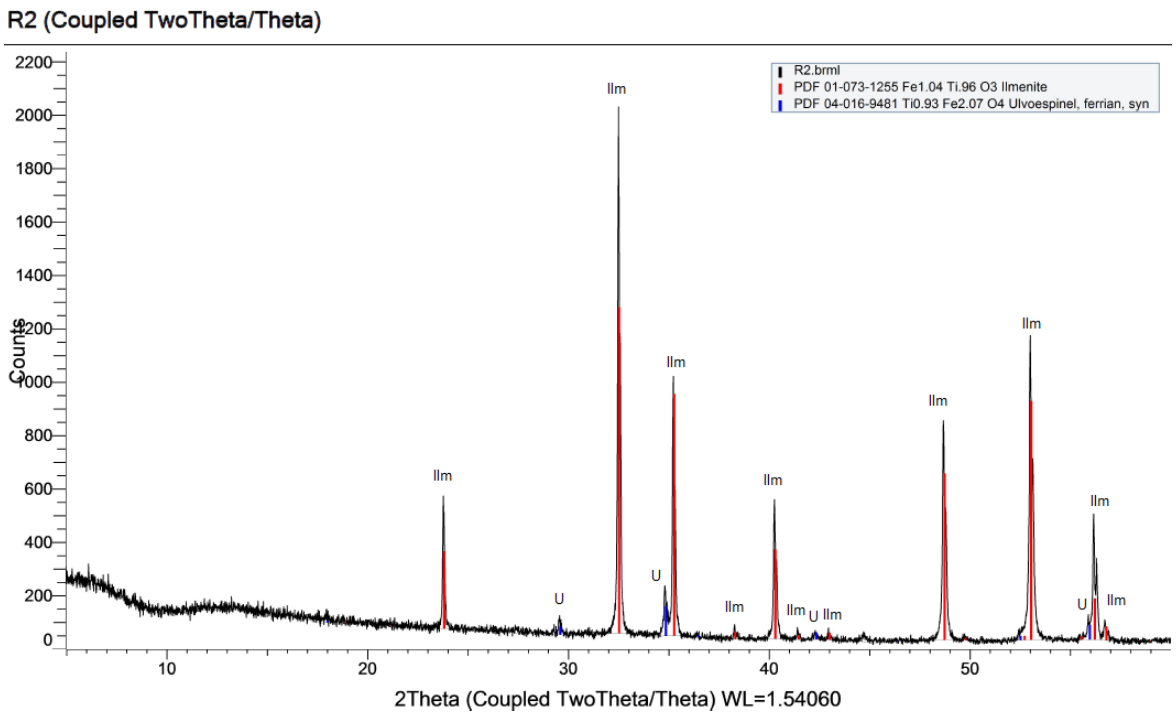

Figure 5.5: X-Ray Diffraction analysis for synthetic ilmenite batch 2.

5.3 Mg-rich ilmenite composition

In Figure 5.6, the XRD results of the Mg-rich ilmenite are shown. Many peaks have been detected, and matched to rutile (reference PDF 04-003-0648, ”R” on the picture), pseudo-brookite (reference PDF 04-007-6638, ”PB” on the picture) and ilmenite (reference PDF 00-029-0733, ”Ilm” on the picture). However, these three phases don’t contain magnesium although magnesium had been introduced on the melt. Two other candidates matched with the set of peaks of the analysed product. These two candidates correspond to an enriched ilmenite phase in magnesium, but are very similar to ilmenite peaks. These candidates’ peaks have been spotted by ” Mg1” (reference PDF 00-027-0247) and ”Mg2” (reference PDF 00-003-0789). The candidates corresponding to Mg_2TiO_5 showed peaks that don’t correspond to those of the analysed product. Thus, they were discarded during the selection process.

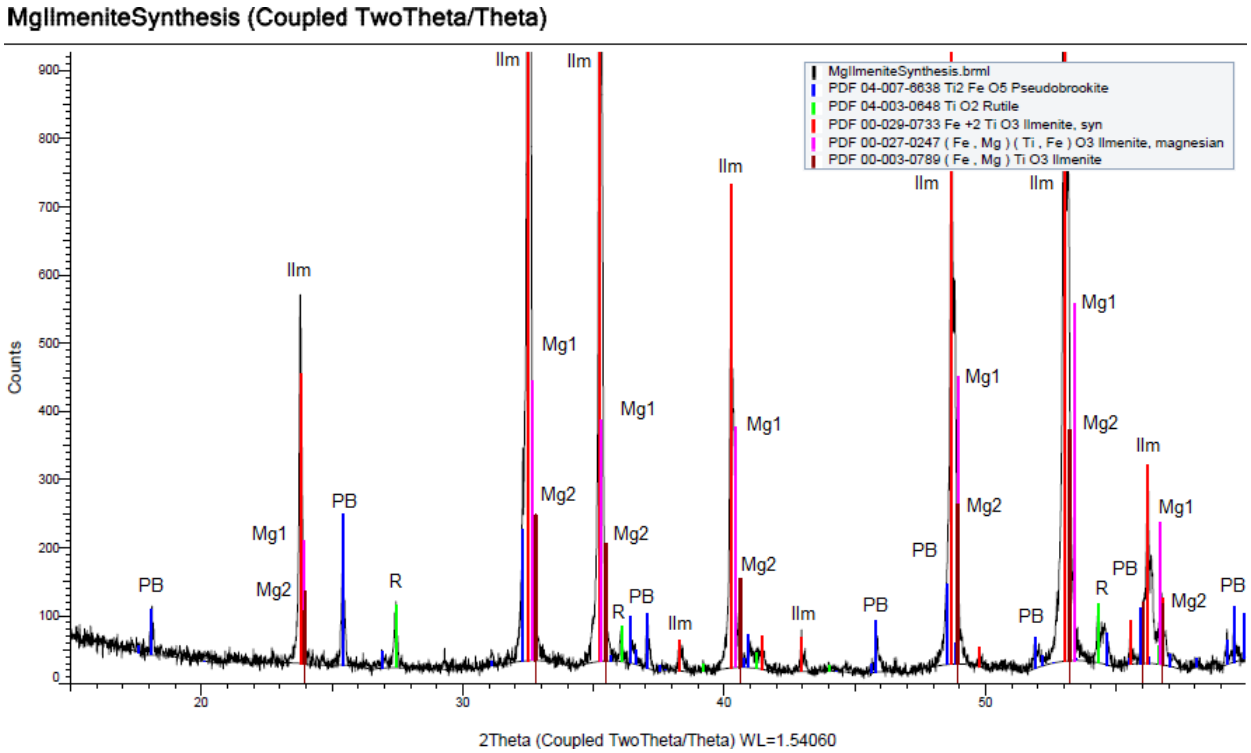

Figure 5.6: X-Ray Diffraction analysis for synthetic Mg-rich ilmenite.

5.4 Pre-oxidized pellets composition

The pre-oxidized ilmenite was reacted according to the temperature curve given in Figure 5.7. Despites the little differences with the targeted temperature in the last measurement, as well as an early one, the measured temperature fits the target well.

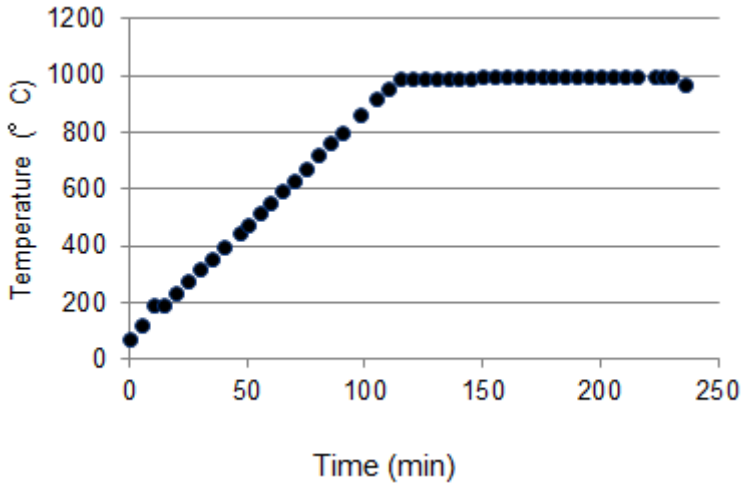

Figure 5.7: Temperature measurement during the pre-oxidation.

The reacted ilmenite pellets' XRD analysis is given in Figure 5.8. Three compounds are evidenced by this graph:

- A first phase detected is pseudobrookite Fe_2TiO_5 with the reference PDF 00-041-1432. The biggest intensity peaks corresponding to this compound are also among the highest of the graph. These are represented in blue and spotted by a "PB" sign.
- The second phase detected in terms of intensity is a rutile phase. The composition given is $Ti_{0.992}O_2$ with the reference PDF 01-086-0148. The intensity peaks for this other compound are the same order of magnitude as those of pseudobrookite. These are represented in red and spotted by a "R" sign.
- The last compound shown in the graph is hematite. Its composition is $Fe_{1.984}O_3$ with the reference PDF 01-077-9925. However, the intensity peaks for this compound are much smaller than those for the other compounds. They are represented in green and spotted by a "H" sign.

Despite no quantitative conclusion possible, these XRD graphs still show that the hematite was in a smaller proportion. The order of magnitude of hematite peaks being

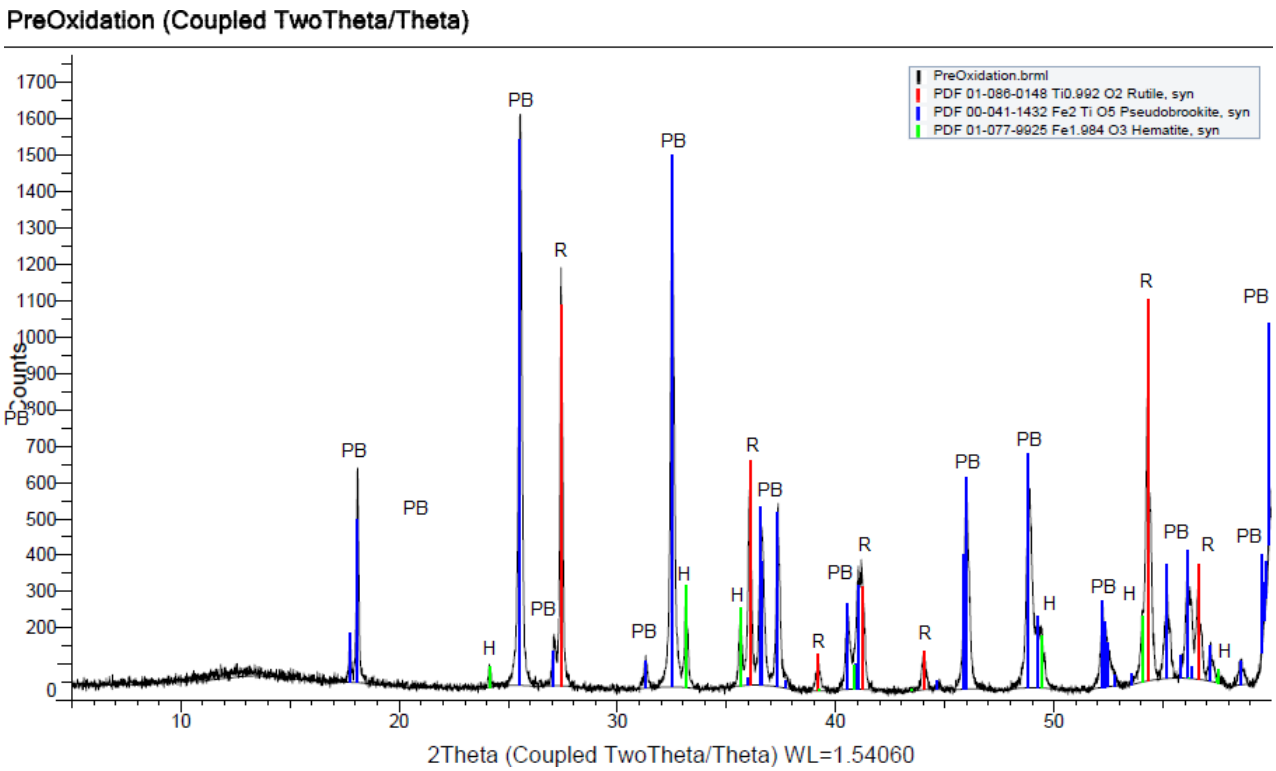

Figure 5.8: X-Ray Diffraction analysis for synthetic ilmenite batch 1.

much smaller, the quantities presented in pre-oxidized pellets is smaller as well. Since the two other compounds show peaks of similar intensity, the product probably contained mostly pseudobrookite and rutile, with some hematite.

/clearpage

5.5 Reduction with H_2 gas

Conversion curve

A first result is the mass curve that has been obtained during the reduction. For practical reasons, this curve has been converted into a "conversion degree" curve. The value 0 in terms of conversion degree corresponds to no mass loss whereas a conversion of 1 corresponds to a loss of 3 oxygen from each couple of Fe_2TiO_5+TiO_2. This curve is shown in Figure 5.9 together with the CO conversion degree curve. A first observation is that this curve, in the case of the H_2, is showing three distinct steps:

- The first step goes from a conversion degree of approximately 0 to 0.35. The speed appears to be almost constant as the curve is close to a straight line. This step is

also the fastest in terms of conversion speed since the conversion degree goes from 0 to 0.35 in approximately 200 seconds.

- The second step goes from a conversion of approximately 0.35 to 1. This step happens right after the first one is done. Again, the curve is almost straight, showing that the reaction speed is constant. This second step is not as fast as the first one, but it's extent is more important as the conversion degree increases by 0.65. The end of this step, however, is difficult to determine. At the end of this second step, some kind of transition goes from about 0.95 to 1.05 of conversion degree. There, the curve is not linear and shows a progressive change in reaction speed.

- The last step goes from approximately 1.05 to 1.14, when the H_2 flow is stopped. Again the speed appears to be constant since the curve is straight in this part. Of all the steps, this one appears to be the slowest. In addition, there is no sign that this reaction wouldn't have continued with more time, since the reaction was still going at a constant speed.

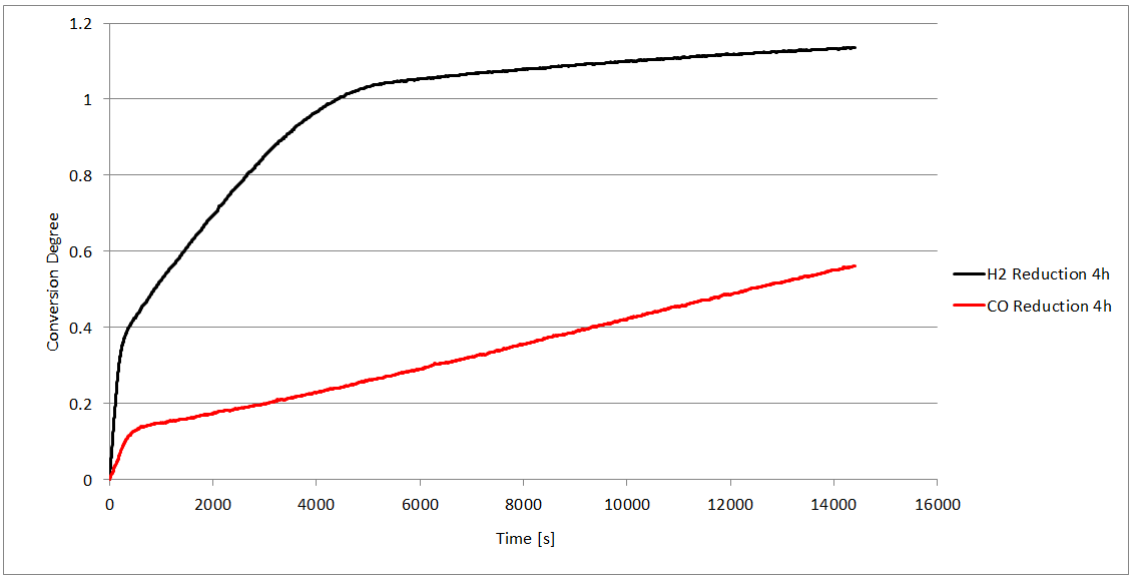

Figure 5.9: Conversion degree curve for CO and H_2 reduction.

XRD analysis

The XRD analyses given in Figure 5.10 provided interesting results on the end product's composition. Two phases were detected, showing that the product contains iron and

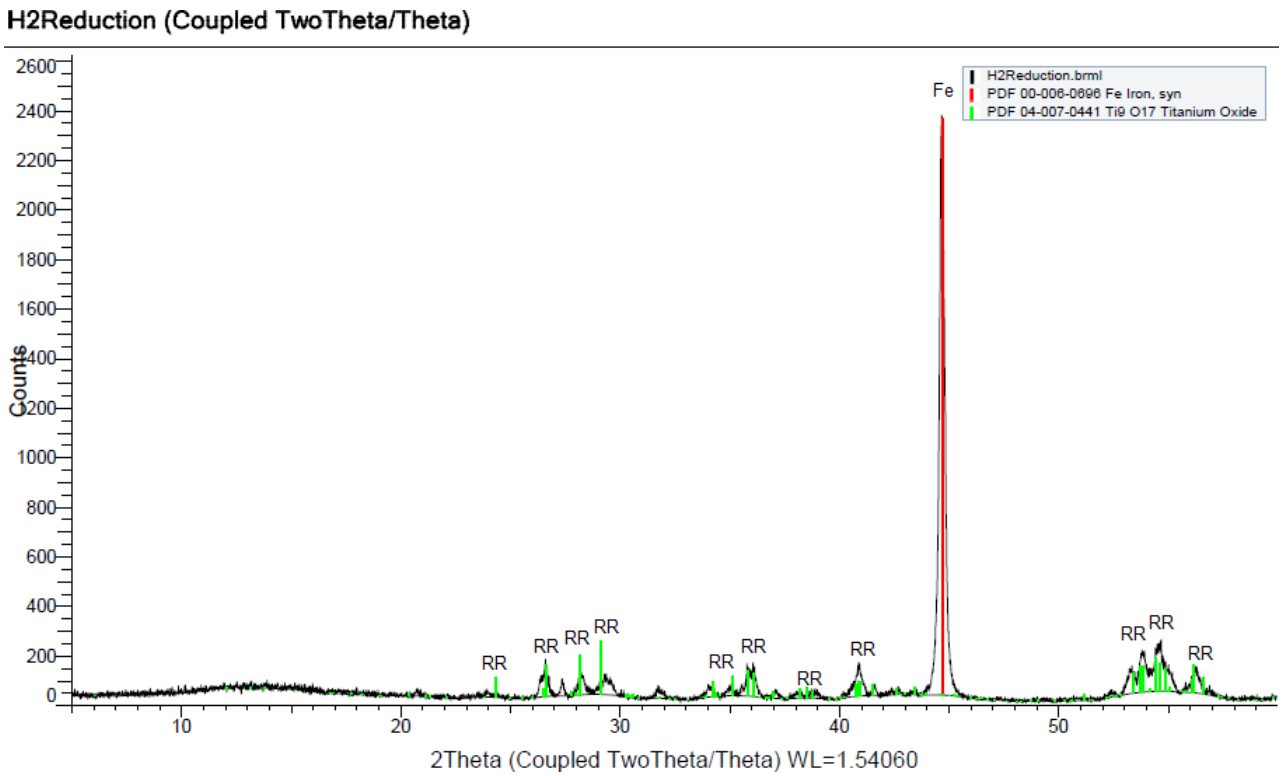

Figure 5.10: X-Ray Diffraction analysis for ilmenite pellets reduced with H_2 gas.

titanium oxide. The iron detected is of reference PDF 00-006-0696, and the peak is unique and intense. Various other peaks corresponding to titanium oxide of reference PDF 04-007-0441 are also shown. This titanium oxide detected is a reduced titanium oxide of formula Ti_9O_{17}, and corresponds to a reduced form of titanium oxide TiO_2. However, the peaks don't all fit perfectly the graph.

Probe micro-analysis

The last series of results from the H_2 reduction is the pictures obtained from electron probe micro-analysis. Three pictures show the same pellet at different depths and at minimum magnification (x500) in Figure 5.11 near the surface, in Figure 5.12 at 2 mm deep, and in Figure 5.13 at 4 mm deep. Looking at these pictures, a first conclusion is that the visual aspect is very similar at all depths. The second picture, taken at 2mm deep, shows more epoxy (in black on the picture). Moreover, in all these pictures, the grey and white phases form small clusters and looks very mixed with each other. The white phase clusters, for example, never exceed a length of 10µm.

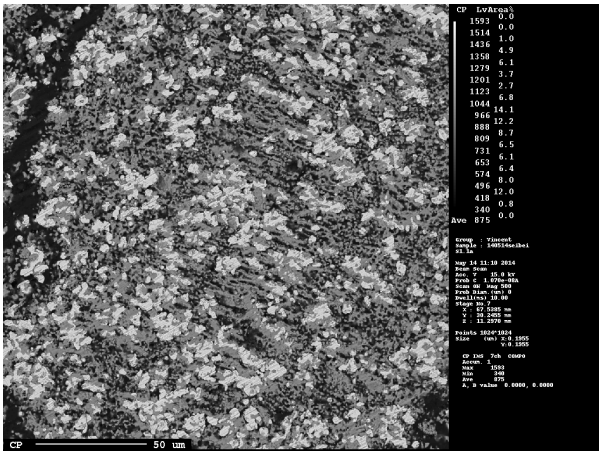

Figure 5.11: Picture of a reacted pellet (with H_2 gas) by EPMA near the surface (x500).

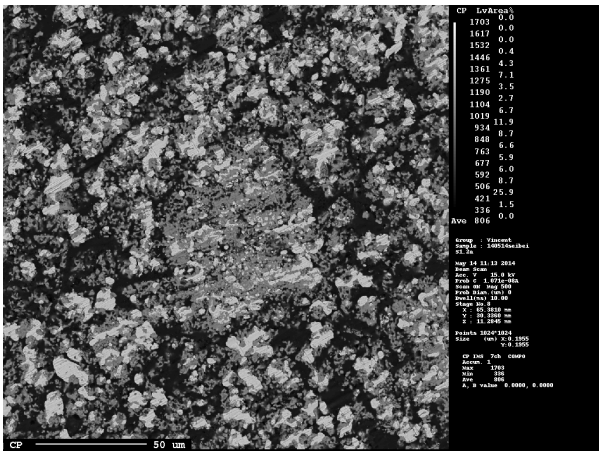

Figure 5.12: Picture of a reacted pellet (with H_2 gas) by EPMA at 2mm deep (x500).

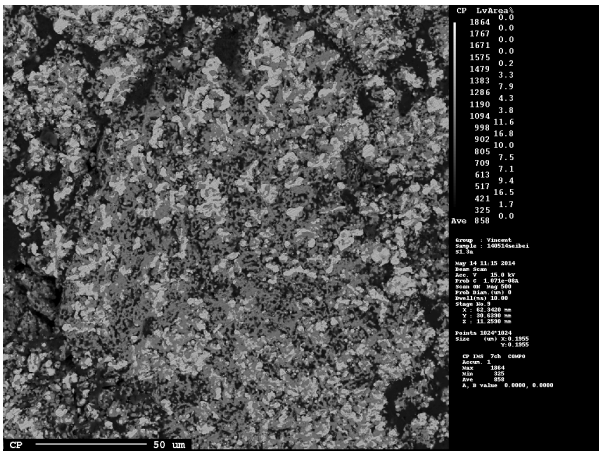

Figure 5.13: Picture of a reacted pellet (with H_2 gas) by EPMA at 4mm deep (x500).

The mapping gives more information about the atomic distribution. In Figure 5.14, the mapping for iron, titanium and oxygen is given. The high magnification allows to see that titanium and oxygen seem to be in the same positions, whereas the iron is in complementary areas. Of course, the black areas that are caused by epoxy, do not contain any of these species.

The quantitative point analysis which has been done on both the white phase and the grey phase reveals that they correspond to iron and titanium oxide respectively. The white phase composition goes from 80% iron to 95% iron approximately, but this deviation might be due to the depth of the analysis, reaching titanium oxide layers below the visible layer. The grey phase shows a titanium to oxygen ratio going from 0.44 to 0.59, which remain close to the 0.50 value corresponding to the ratio for TiO_2. However, contrary to the XRD results given before, this analysis does not give the structure of the titanium oxide. The results in terms of atomic proportions are given in Table 5.1. The pictures from micro-analysis are fully given in appendix, together with the pictures and positions of the points' analyses.

The naming is done as such:

- S1 or S2 corresponds to the experiment (S1 for H_2 reduction, S2 for CO reduction)
- The following number "1", "2" or "3" corresponds to the depth "1" being the surface, "2" being 2 mm deep, and "3" being 4 mm deep.
- The letter corresponds to the magnification, "a" for x500, "b" for x1000 and "c" for x2000.

- The last number corresponds to a position on the picture.
- The corresponding pictures are given in Figure 5.15- 5.17

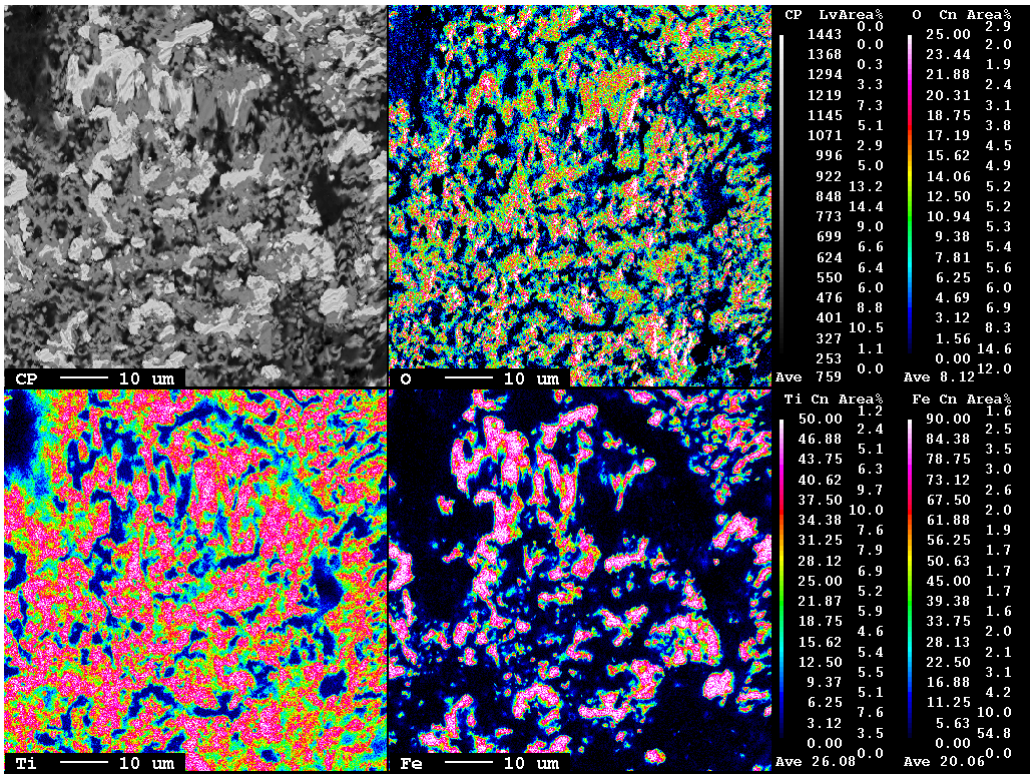

Figure 5.14: Mapping of iron, titanium and oxygen in an ilmenite pellet reacted with H_2 at 4 mm deep (x2000).

Table 5.1: Atomic proportions of Ti, Fe and O given by quantitative point analysis on an ilmenite pellet reduced with H_2 gas.

No.	O	Ti	Fe	Total	Picture name
1	10.0737	9.1759	80.7503	99.9999	S1.1c.1
2	2.4017	4.3192	93.2791	100	S1.1c.2
3	1.2317	4.6126	94.1557	100	S1.1c.3
4	65.3658	33.7061	0.9282	100	S1.1c.4
5	65.2834	33.9224	0.7942	100	S1.1c.5
6	64.2042	35.0842	0.7116	100	S1.1c.6
7	3.0157	4.0218	92.9625	100	S1.2c.1
8	1.6294	3.5048	94.8658	100	S1.2c.2
9	1.1622	3.5056	95.3323	100	S1.2c.3
10	66.7028	32.3759	0.9213	100	S1.2c.4
11	63.1779	35.9964	0.8257	100	S1.2c.5
12	61.8939	27.5731	10.533	100	S1.2c.6
13	1.3853	4.1808	94.4339	100	S1.3c.1
14	2.3361	4.265	93.3989	100	S1.3c.2
15	2.1112	4.3435	93.5453	100	S1.3c.3
16	65.0653	34.0834	0.8514	100	S1.3c.4
17	62.2074	36.9259	0.8667	100	S1.3c.5
18	63.7251	34.8207	1.4541	100	S1.3c.6

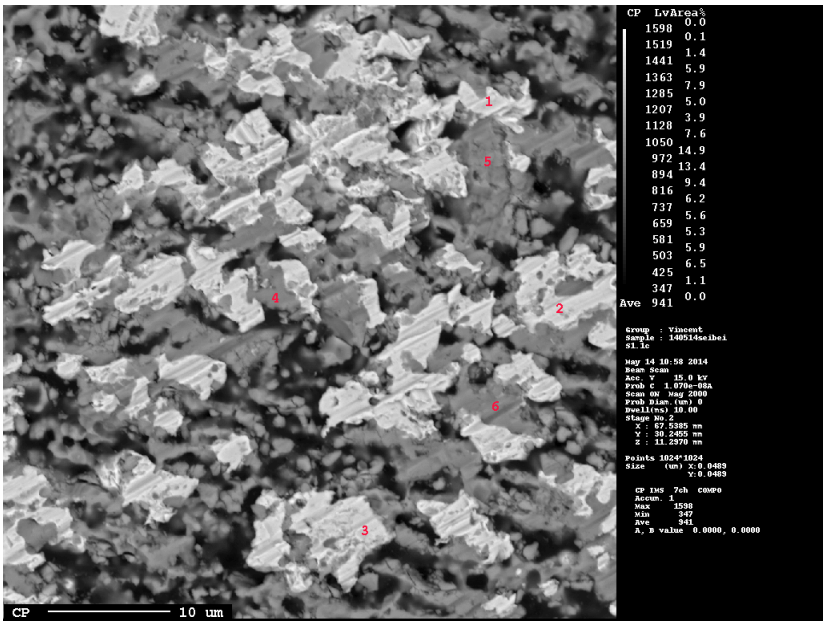

Figure 5.15: Quantitative point analysis positions in an ilmenite pellet reacted with H_2 at the surface (x2000).

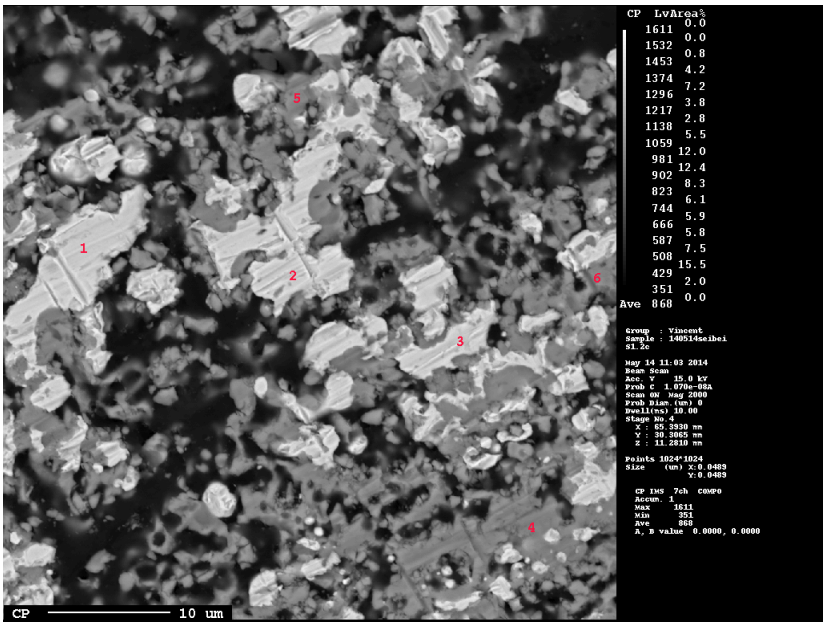

Figure 5.16: Quantitative point analysis positions in an ilmenite pellet reacted with H_2 at 2 mm deep (x2000).

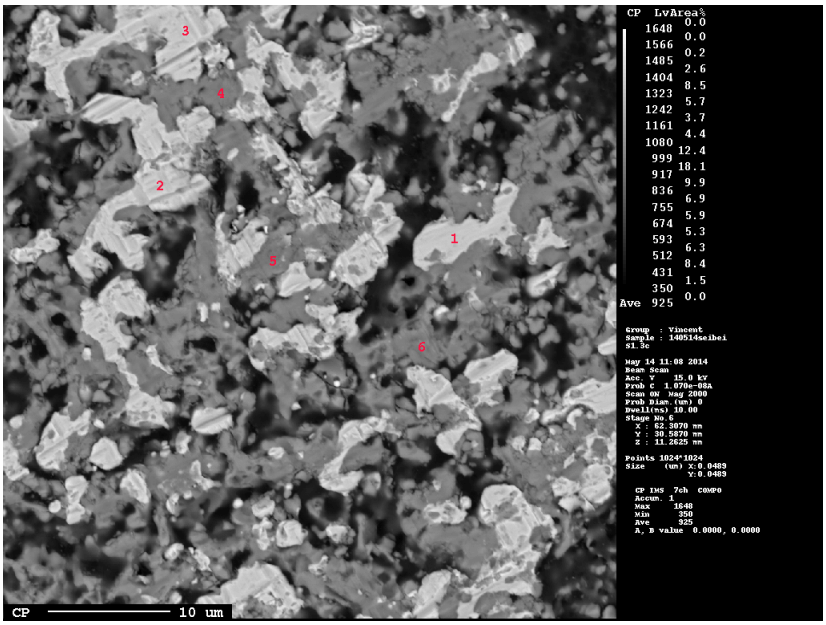

Figure 5.17: Quantitative point analysis positions in an ilmenite pellet reacted with H_2 at 4 mm deep (x2000).

5.6 Reduction with CO gas

Conversion curve

The mass curve obtained during the experiment is again converted to a "conversion degree" curve. This curve is shown in Figure 5.9 given before. In this experiment, only two steps are noticeable :

- The first step goes from a conversion degree of approximately 0 to 0.13. The speed looks constant since the curve is approximatively a straight line. This step is the fastest by far in terms of conversion speed. A break in the curve limits this step between 0.13 and 0.15 of conversion degree.
- The second step goes from a conversion of approximately 0.15 to 0.56. Again, the reaction speed seems constant. This second step is not as fast as the first one, but it's extent is more important as the conversion degree increases by 0.41. As before in the H_2 reduction experiment, the gas flow is stopped. Again, there is no sign that this reaction wouldn't have continued with more time because is keeping the same speed.

XRD analysis

The XRD graph is given in Figure 5.18. Three phases are detected: iron, titanium oxide and ilmenite. The iron detected is of reference PDF 04-007-9753, with a unique and strong peak. The remaining peak of medium to small size compared with the iron peak, corresponds to ilmenite of reference PDF 01-073-1255 spotted by "Ilm" and rutile of reference PDF 01-086-0148 spotted by "R". Contrary to the graph for H_2 reduction, the rutile is here in a non reduced state, with formula $Ti_{0.992}0_2$.

Probe micro-analysis

The following pictures are obtained from electron probe micro-analysis of ilmenite pellets reduced with CO gas. Three pictures shows the same pellet with at different depths and at minimum magnification (x500) in Figure 5.19 near the surface, in Figure 5.20 at 2 mm deep, and in Figure 5.21 at 4 mm deep.

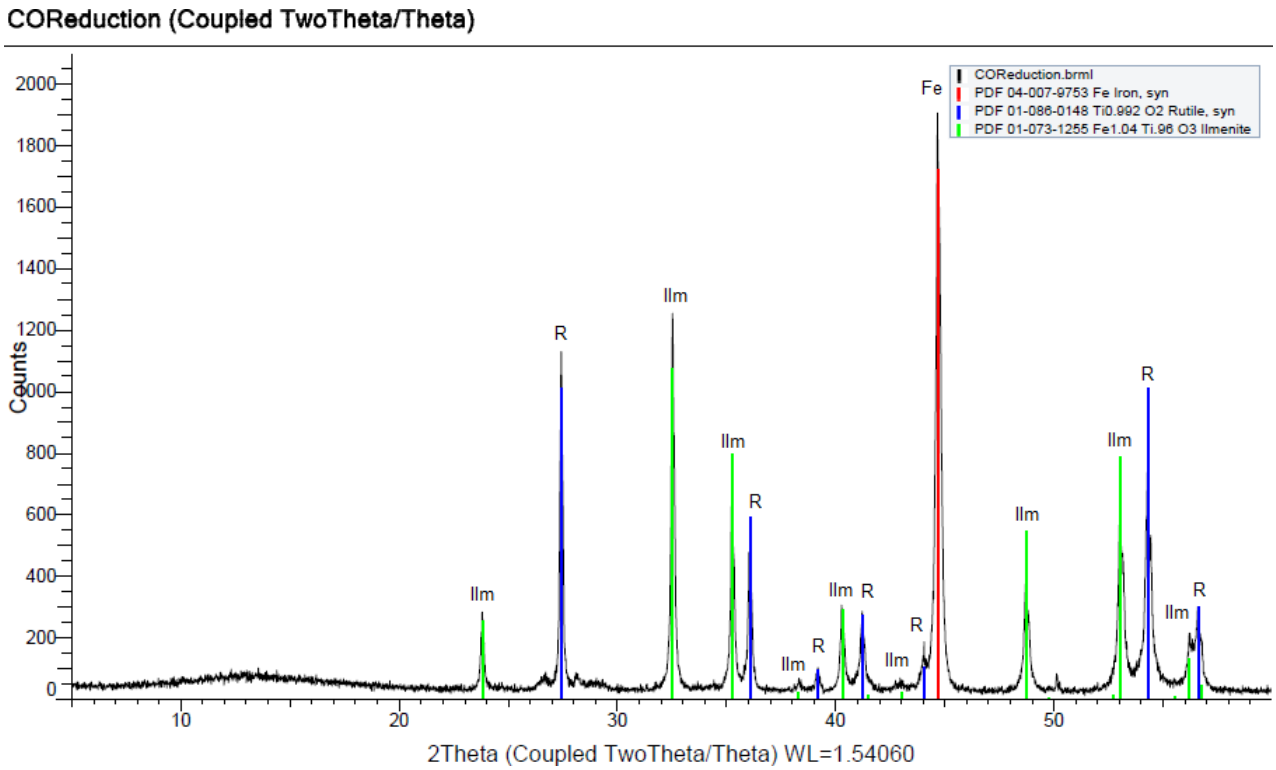

Figure 5.18: X-Ray Diffraction analysis for ilmenite pellets reduced with CO gas.

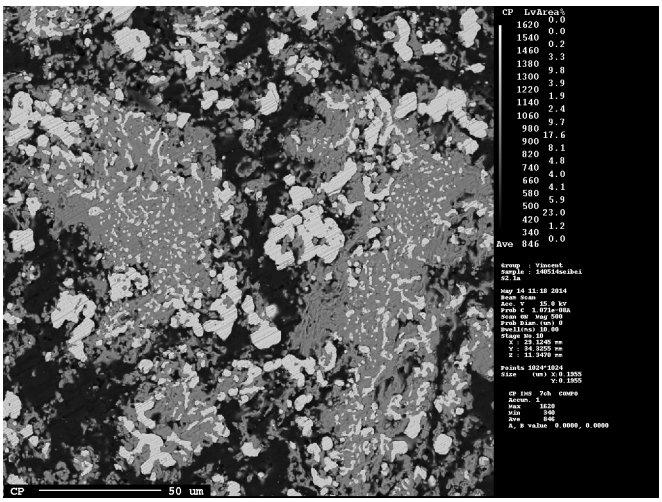

Figure 5.19: Picture of a reacted pellet (with CO gas) by EPMA near the surface (x500).

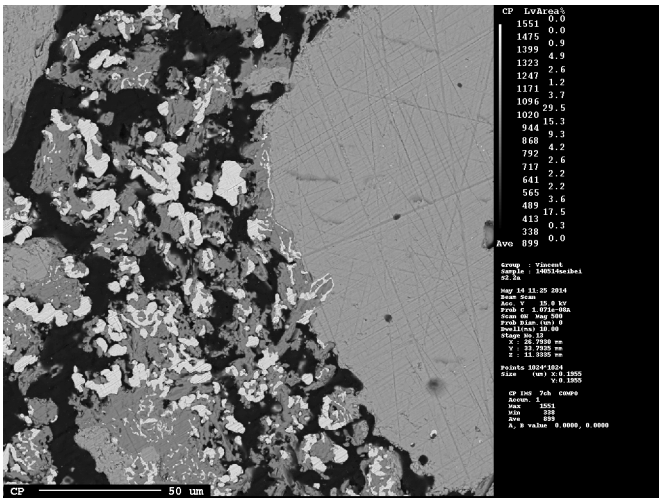

Figure 5.20: Picture of a reacted pellet (with CO gas) by EPMA at 2mm deep (x500).

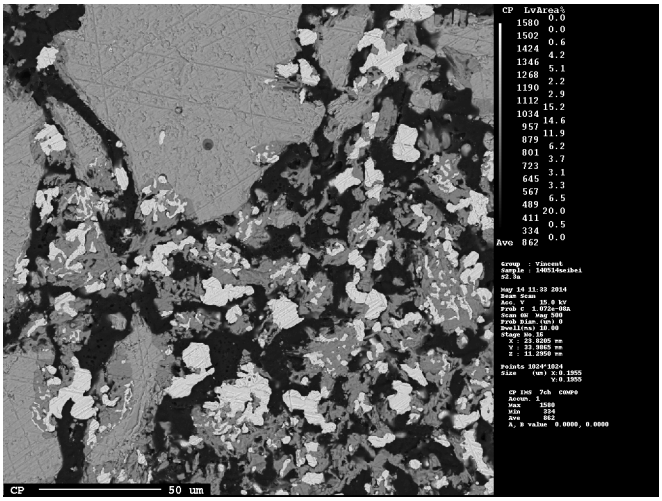

Figure 5.21: Picture of a reacted pellet (with CO gas) by EPMA at 4mm deep (x500).

A first observation from these pictures is that the clusters of dark grey and white phases are sometimes bigger than in the H_2 experiment. In addition, three different colors are detected in addition to the black due to epoxy. White and dark grey areas are mixed together. Also, large light grey areas are showed only in the two last pictures, deeper in the pellet. In Figure 5.20 and Figure 5.21, these light grey phases are in contact with a mix of the two other phases. This seems to happen only on the edges to form a layer, and not inside the light grey areas.

In Figure 5.22, the mapping of the different chemical elements involved is given. On the picture, it is clear that a particular phase is present on the right side. Moreover a layer is formed on the edges of this phase, containing titanium and oxygen on some clusters, and iron in the others. This layer is not only in contact with the light grey phase, but seems to penetrate it. The phase on the right side contains iron, oxygen and titanium.

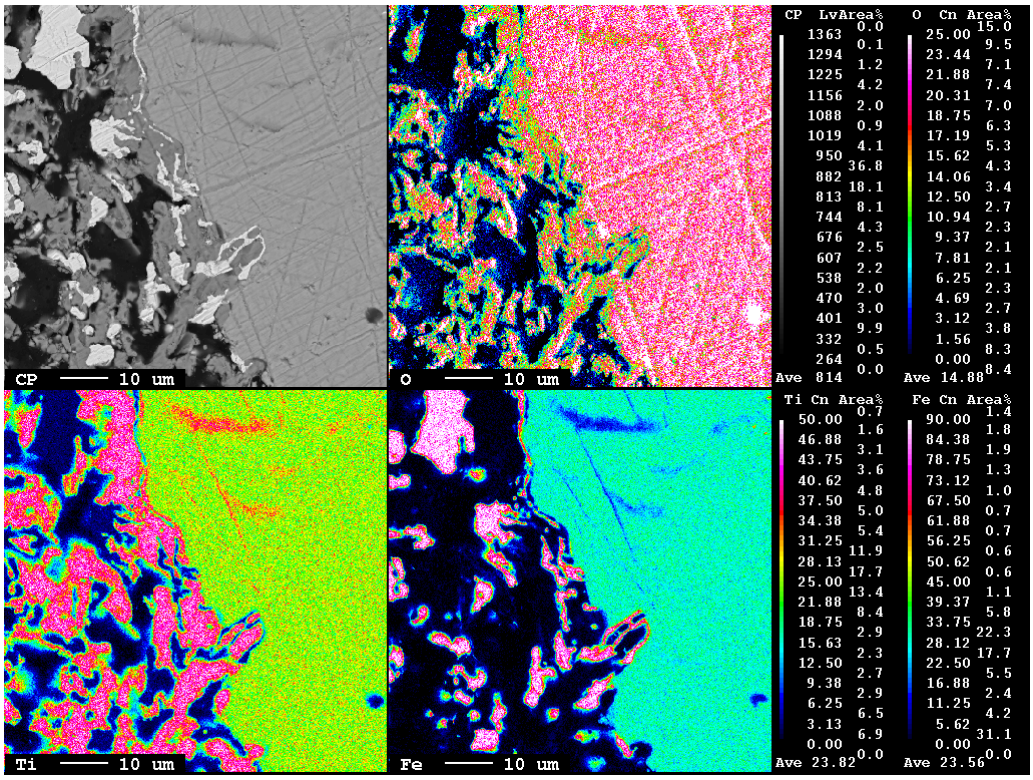

Figure 5.22: Mapping of iron, titanium and oxygen in an ilmenite pellet reacted with CO at 2 mm deep (x2000).

The quantitative point analysis reveals the compositions of the different phases. Thus, the white phase and dark grey phase corresponds to iron and titanium oxide respectively.

The light grey phase which was not present in the H_2 experiment, has approximatively the atomic composition of ilmenite. The results in terms of atomic proportions are given in Table 5.2. Concerning the white phase, the molar percentage of iron varies from 93.46% to 95.99% showing the dominance of iron in this phase.The dark grey phase is clearly titanium oxide. However, the titanium/oxygen ratio varies from 0.45 to 0.53. The last phase's composition is varying around 60% oxygen, 20% titanium and 20% iron.

Table 5.2: Atomic proportions of Ti, Fe and O given by quantitative point analysis on an ilmenite pellet reduced with CO gas.

No.	O	Ti	Fe	Total	Picture name
19	1.4713	3.2343	95.2944	100	S2.1c.1
20	1.359	3.0838	95.5572	100	S2.1c.2
21	1.3237	3.257	95.4193	100	S2.1c.3
22	68.7677	30.7741	0.4582	100	S2.1c.4
23	67.5446	31.742	0.7134	100	S2.1c.5
24	67.6936	31.4324	0.874	100	S2.1c.6
25	2.0522	2.8778	95.07	100	S2.2c.1
26	2.978	3.133	93.8891	100	S2.2c.2
27	2.7421	2.2477	95.0103	100	S2.2c.3
28	65.7465	33.6277	0.6258	100	S2.2c.4
29	67.7347	31.6892	0.5761	100	S2.2c.5
30	64.6766	34.605	0.7184	100	S2.2c.6
31	60.3428	20.415	19.2422	100	S2.2c.7
32	60.6075	20.2982	19.0943	100	S2.2c.8
33	61.6938	20.4456	17.8606	100	S2.2c.9
34	1.3793	2.6299	95.9908	100	S2.3c.1
35	2.4352	2.5159	95.0489	100	S2.3c.2
36	3.4095	3.126	93.4645	100	S2.3c.3
37	66.5193	32.8954	0.5853	100	S2.3c.4
38	65.4096	33.857	0.7333	100	S2.3c.5
39	67.8941	31.5496	0.5563	100	S2.3c.6
40	61.3413	20.0347	18.6241	100	S2.3c.7
41	58.6539	21.3115	20.0346	100	S2.3c.8
42	63.1659	18.8863	17.9478	100	S2.3c.9

The corresponding pictures are given in Figure 5.23- 5.25

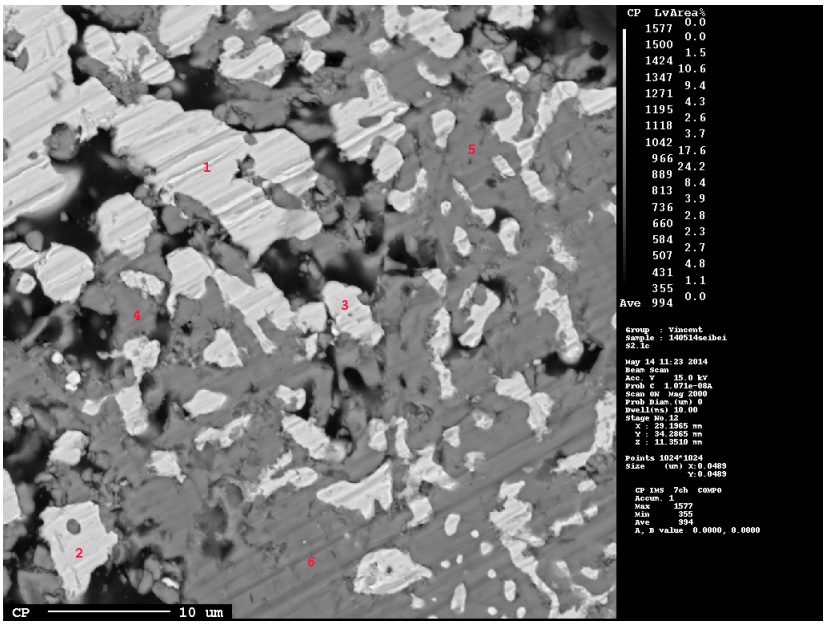

Figure 5.23: Quantitative point analysis positions in an ilmenite pellet reacted with CO at the surface (x2000).

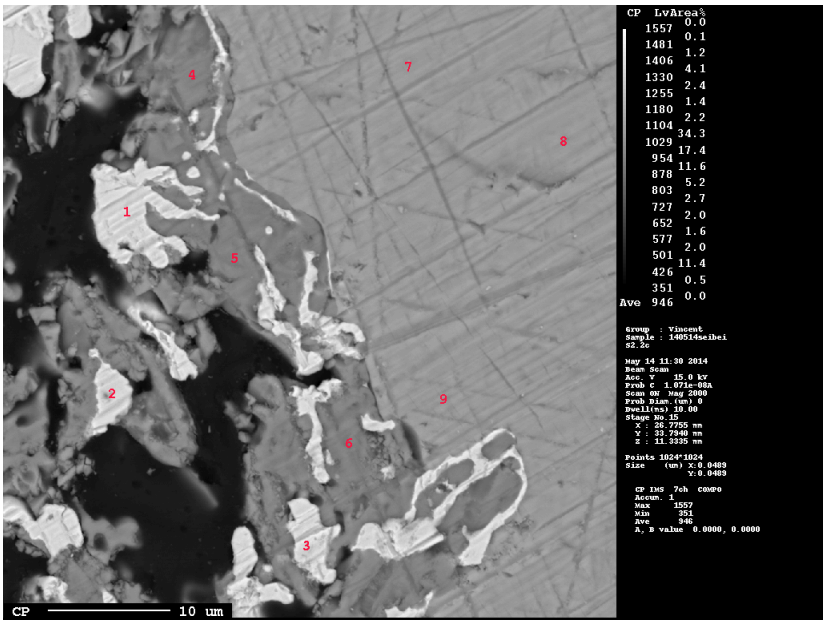

Figure 5.24: Quantitative point analysis positions in an ilmenite pellet reacted with CO at 2 mm deep (x2000).

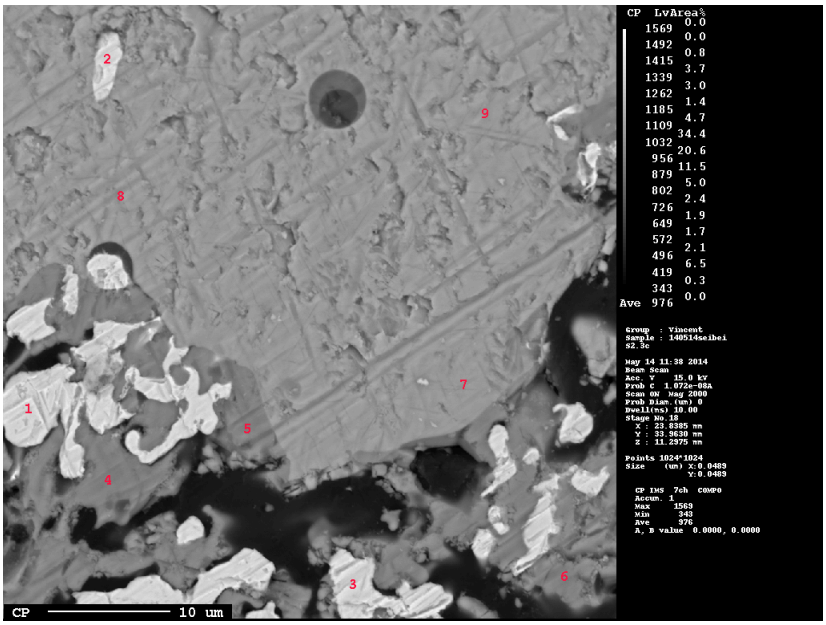

Figure 5.25: Quantitative point analysis positions in an ilmenite pellet reacted with CO at 4 mm deep (x2000).

Chapter 6

Discussion

6.1 Synthesis of ilmenite and Mg-rich ilmenite

Pure ilmenite synthesis

The synthesis of ilmenite aimed at producing a pure synthetic ilmenite while avoiding impurities as much as possible. The impurities detected with the XRD analyses were TiO_2 and Fe in one batch and Fe_2TiO_4 in the second. Both batches also presented a crusts on the top and iron pieces in the bottom of the crucible.

The theory points presented earlier explain these impurities. Although the compounds have been introduced in the stoichiometric composition of ilmenite ($FeTiO_3$), a crust was left on the top of the crucible. Because the pure iron is unlikely to have stayed in such a crust due to induction effects, this crust likely changed the stoichiometry by being only made up of iron oxide and titanium oxide. The pieces of iron found in the bottom of each experiment are sort of compensating for this, and is justified by the fact that iron is likely to be expelled during cooling. Moreover the composition of the crust has no reason to follow the ratio of 3 TiO_2 for each Fe_2O_3, initially introduced. Indeed, the crust could contain either excess TiO_2 or excess Fe_2O_3. Looking at the ternary diagram of Fe-Fe_2O_3-TiO_2 presented earlier, the Fe_2TiO_4 forming is explained by an excess of TiO_2 in the crust. The TiO_2 and Fe forming in ilmenite are due to, on the contrary, an excess of Fe_2O_3 in the crust.

The forming of a crust has been observed in many experiments, but is not found to be due to thermodynamic causes. Indeed, with a better positionning of the iron on the

top of the melt this crust is avoided. The Mg-rich ilmenite synthesis experiment showed no crust formation when the iron pieces were spread on the top of the raw materials, to melt the top layer.

All in all, the composition of the ilmenite produced follows the ternary diagram studied well. However the particle size distribution obtained after crushing has not been controlled during the synthesis. Since this parameter may play an important role in further chemical reactions, an enhancement of the process, maybe through a different cooling path influencing the porosity, is to look closer.

Mg-rich ilmenite synthesis

Concerning the synthesis of Mg-rich ilmenite, the main aim was to ensure the capture of Mg atoms in the ilmenite structure. In addition, the composition obtained had to contain as little undesired other phases as possible. The XRD analyses showed that the main product of the synthesis was an ilmenite phase. This could very well be ilmenite containing magnesium since the peaks overlap with iron titanium oxide ($FeTiO_3$). Since no other phases detected contained magnesium, and given that magnesium is unlikely to leave the melt, it is reasonable to assume that and $FeTiO_3$-$MgTiO_3$ phase has been formed.

The pseudobrookite phase found might be due to the excess rutile used during this experiment. Originally, this excess rutile was used to prevent the forming of M_3O_4 phases, but seems to have favored the production of pseudobrookite.

Finally, the splashing that happened during the experiment might be due to the use of raw materials containing moisture, or to a wrong placement of the reactants. A possible improvement could be the drying of the raw materials, as well as a mixing of the mangesium oxide with the two others (titanium and iron oxides) in the lower part of the crucible.

This Mg-rich ilmenite sythesis appears to be succesful and some undesired phases have been avoided. However, there is still room for improvements such as the avoiding of pseudobrookite formation. In terms of experimental protocol, the placement and handling of raw materials could be improved in order to avoid splashing.

6.2 Pre-oxidation of ilmenite pellets

As observed in the product after pre-oxidation, pseudobrookite, hematite and rutile have been formed. Due to the reactions presented before, the pseudobrookite and rutile production is explained by sintering at temperatures higher than 800°C. However because the pellets have been introduced at ambient temperature, and therefore underwent the rise of temperature, ilmenite has reacted at temperatures lower than 800°C giving hematite and rutile. To limit this effect and investigate the impact of the pre-oxidation for pure synthetic ilmenite reduction, the reactants could be introduced at 800°C or even 1000°C. This is particularly important if hematite and pseudobrookite are reduced differently later on. However, this might compromise the strengh of the pellets because of thermal shock.

6.3 Reduction of ilmenite pellets with H_2 gas

Reactions and extent

The results from the mass loss curve, converted into a conversion degree curve, clearly show three steps. Because the breaks in the curve happen approximatively at 0.33 and 1 of conversion degree, and given the composition of the starting material and the reactions reported by other works, it is possible to imagine the reduction as follows.

The first part, from a conversion degree of 0 to a value around 0.33 corresponds to the reduction from iron (III) to iron (II). Different phases were found in pre-oxidized pellets: hematite with rutile and pseudobrookite with rutile, but both correspond to iron (III) oxides. Since a complete conversion from iron (III) to iron (II) would give a conversion degree appoximately of 0.33, it is reasonable to consider that this first step ends when the pellets only contain iron (II) oxides. Others works note that ilmenite is reformed at this step, but more analysis is needed in this case. Indeed, because the XRD graphs and micro-analyses only give information on the end product, further investigations requires to analyse partially reacted pellets .

The second step, from a conversion degree of approximately 0.33 to 1 corresponds to the reduction of iron (II) to iron metal. It is clear in the XRD and EPM analyses that metallic iron was obtained. A full reduction from iron (III) to iron (II) followed by a full reduction of iron (II) to iron metal corresponds to a conversion degree of 1.

The third and last step seems unfinished. The conversion curve indeed shows a constant conversion rate even in the last section of the experiment. No signs of flattening were observed. Because of the composition of the initial materials, and because of the products observed by XRD, it is possible to assume that all the iron was reacted at the end. Even though, the reaction was still going and the rutile observed shows a reduced state. These signs show that reduction of rutile was going after the reduction of iron. This also explains that the conversion degree goes further than 1. Indeed, more than three oxygen are lost for each couple of Fe_2TiO_5+TiO_2.

From these analyses, it is possible to assume that the reduction of iron (II) starts after the reduction of iron (III) because the extent, in terms of conversion degree and because of the clear change in reduction speed. Also, it is possible to consider that the reduction of titanium oxide starts when all the iron is reduced to iron metal. This could be confirmed experimentaly by repeating the same experiment multiple times, but by stopping the reduction process by shutting down the H_2 gas supply. Analysis on the structures and the phases involved would give information on the actual processes.

Gas-solid reactions

Even if only the final picture is given by the analyses, the reaction of the solid with H_2 gas shows particular features.

First, it must be noted that the pellet looked uniform throughout after the reaction with H_2 gas. It is indeed not possible to distinguish areas that initially contained pseudo-brookite to those containing hematite from the final picture. Second, the clusters of iron obtained after the reaction tend to be of small size, generally below 10 µm of diameter. Thus, iron and reduced rutiles are very mixed. Because of that, it is possible to assume that the penetration of H_2 gas into the particle as well as the exhausting of H_2O was fairly easy and formed iron and reduced rutile everywhere. No remaining unreacted core was found because the reaction was stopped after all the iron was converted. Since there is no contrary arguments, the Progressive-Conversion Model could be an accurate way to describe the reduction reaction with H_2 gas. To investigate more on this, stopping the reaction would be again accurate: it would allow to see whether or not an unreacted core is present during the reaction.

6.4 Reduction of ilmenite pellets with CO gas

Reactions and extent

The results from the reduction experiment with CO are much more difficult to explain. The conversion degree curve shows only two different steps, and one break. This time, the break is happening at approximatively 0.13 of conversion.

First, a fast reduction step initiates the reduction of the pellets. This reaction is going from a conversion degree of 0 to approximately 0.13. Because the iron present is trivalent, and because titanium was not reduced according to the XRD analysis, this step looks to be the reduction from iron (III) to iron (II) of a part of the iron. The reasons why the speed of the reaction is changed at some point may be a forming of an iron shell around the particle or difficulties for the reacted gas to leave the particle.

The second step is initiated after a conversion degree of 0.13. This step shows a constant reaction speed but the experiment is stopped before the end of this step. Nothing indicates that the reaction would have stopped by itself at this level, since the reactions seemed to be continuing. Because of the reactions presented before as theoretical background, and because of the XRD results, both reduction from iron (III) to iron(II) and iron (II) to iron metal seem to happen at this step. The unreacted materials left are ilmenite, which shows that at some point, all iron (III) was reduced into iron (II). The presence of iron (III) in two types of material after oxidation, hematite and pseudobrookite, might explain this phenomenon. However, more experiments showing the pellets during the reaction are needed to know exactly how the reduction behaves.

From these analyses, it is possible to assume that the reduction of iron (II) starts during the reduction of iron (III) because the extent of the first step in terms of conversion degree. However, the reduction of iron (III) is completed at the end of the experiment, and seemed to be favored. Again, analysis on the structures and the phases present at different times during the experiment would help to explain the different reactions.

Gas-solid reactions

Thanks to the pictures from EPMA, it is clear that an unreacted core is formed during the reduction or iron (II) into iron metal. Because there is only information on the final product, it is not possible to detail the iron (III) reduction reaction.

The unreacted iron (II) core seems to be surrounded by a product layer, containing both iron metal and titanium oxide. Also, the clusters of these materials seem bigger than with the H_2 gas reduction. Unfortunately, is it not possible to state which step is limiting, regarding the shrinking core model. However, it is possible to imagine experiments answering these questions.

Indeed, many parameters could be changed to investigate the gas-solid reaction. A change in the gas flow could show that the diffusion through the gas layer is limiting. A change in temperature could help to investigate the speed of the chemical reaction. Finally, the impact of the particle size distribution could be studied using different particle sizes.

Chapter 7

Conclusion

Two different syntheses were investigated: the synthesis of pure ilmenite, and the synthesis of Mg-rich ilmenite. These syntheses carried out with the cold crucible induction furnace showed to be satisfactory in terms of quality, quantities produced and reproducibility of the experiments. Moreover, the impurities found proved to be expected and explainable. The Mg-ilmenite synthesis is also showing promising results.

Two reduction experiments were also carried out, testing two reducing gases: H_2 and CO gas. Although the H_2 gas reduction shows three distincts steps explained by the XRD analysis and the EPMA, the CO reduction showed unexpected results. Indeed, the reduction sequence with H_2, iron(III) to iron (II) reduction, iron (II) to iron metal and reduction of titanium oxide is not clearly identified in the CO reduction experiments. The potential causes identified mostly are the particle size and the pre-oxidation of the pellets.

To investigate the reduction mechanisms, stopping the reaction is suggested. By stopping the reducing gas flow during the experiment at chosen times, the complete picture could be obtained.

With this work, the synthesis of ilmenite by melting has been sucessfuly developed. Possible improvement based on the present results are also proposed to reach even better results. The reduction reactions studied showed an important difference between the two gases and support the need for deeper investigations.

Chapter 8

Future work

This work is an opening on various new investigations. The melting route for synthetic ilmenite, although fitting the expectations, could be improved. This is particularly true for synthesis of ilmenite with chosen impurities, in addition to Mg, and would help to reach an even better purity. Different impurities could be added, and even a mix of impurities, to investigate the effect other species in ilmenite.

This also applies to the reduction experiments. These compositions could be tested to see in practice the impact of the impurities. In addition, the reduction processes could also be investigated by stopping the experiments at different times to better understand how the particles are reacted. This way, it will be possible in the end to model the gas-solid reactions.

Bibliography

Ackland, M. (2011). The Grande Côte mineral sands project. *Eighth International Heavy Minerals Conference, Perth.*

Borowiec, K. and Rosenqvist, T. (1981). Phase relations and oxidation studies in the system Fe-Fe_2O_3-TiO_2 at 700-1100°C. *Scandinavian Journal of Metallurgy*, 10:217–224.

Borowiec, K. and Rosenqvist, T. (1985). Phase relations and oxygen potentials in the Fe-Ti-Mg-O System. *Scandinavian Journal of Metallurgy*, 14:33–43.

Canaguier, V. (2013a). Synthesis of ilmenite – techniques and challenges. *Norwegian University of Science and Technology, Department of Materials Science and Engineering.*

Canaguier, V. (2013b). Synthesis of ilmenite ($FeTiO_3$). *Master's Project, Norwegian University of Science and Technology, Department of Materials Science and Engineering.*

Charlier, B., Duchesne, J.-C., and Vander Auwera, J. (2006). Magma chamber processes in the Tellnes ilmenite deposit (Rogaland anorthosite province, SW Norway) and the formation of Fe-Ti ores in massif-type anorthosites. *Chemical Geology*, 234:264–290.

Charlier, B., Skår, Ø., Korneliussen, A., Duchesne, J.-C., and Vander Auwera, J. (2007). Ilmenite composition in the Tellnes Fe–Ti deposit, SW Norway: fractional crystallization, postcumulus evolution and ilmenite–zircon relation. *Contributions to Mineralogy and Petrology*, 154(2):119–134.

Elliott, J. F., Gleiser, M., and Ramakrishna, V. (1963). Thermochemistry for steelmaking - thermodynamic and transport properties.

Folmo, G. and Rierson, D. W. (1992). Ilmenite direct reduction project in Norway using the Grate-Car process. *Ironmaking Conference Proceedings*, 51:451–457.

Grey, I. E., Reid, A. F., and Jones, D. G. (1974). Reaction sequences in the reduction of ilmenite: 4. Interpretation in terms of the Fe-Ti-O and Fe-Mn-Ti-O phase diagrams . *Transactions of the Institution of Mining and Metallurgy*, 83(811):C105–11.

Gupta, S. K., Rajakumar, V., and Grieveson, P. (1991). Phase transformations during heating of ilmenite concentrates. *Metallurgical Transactions B*, 22(5):711–716.

Hussein, M. K., Kammel, R., and Winterhager, H. (1967). A study on the reduction mechanism of ilmenite ores. *Indian Journal of Technology*, 5(December):369–377.

Jones, D. G. (1973). Reaction sequences in the reduction of ilmenite. 2. Gaseous reduction by carbon monoxide. *Transactions / Institution of Mining and Metallurgy. Section C*, 82:186–192.

Levenspiel, O. (1999). Chapter 25 Fluid-particle reactions: kinetics. *Chemical Reaction Engineering*, pages 566–588.

Lindsley, D. H. (2003). Do Fe-Ti oxide magmas exist? Geology: yes; Experiments: no! *Special Publication*, 9:34–35.

Lobo, S., Kolbeinsen, L., and Seim, S. Reduction of ilmenite with synthesis gas. *Heavy minerals conference 2013*.

Pang, K.-N., Zhou, M.-F., Lindsley, D., Zhao, D., and Malpas, J. (2008). Origin of Fe–Ti oxide ores in mafic intrusions: evidence from the Panzhihua Intrusion, SW China. *Journal of Petrology*, 49(2):295–313.

Philpotts, A. R. (1967). Origin of certain iron-titanium oxide and apatite rocks. *Economic Geology*, 62(3):303–315.

Pistorius, P. C. (2003). Fundamentals of freeze lining behaviour in ilmenite smelting. *South African Institute of Mining and Metallurgy*, 103:509–514.

Seim, S. (2011). Experimental investigations and phase relations in the Liquid $FeTiO_3$-Ti_2O_3-TiO_2 slag system. *Norwegian University of Science and Technology, Department of Materials Science and Engineering*, (2011:105).

Solheim, J. J. (1988). The Tyssedal ilmenite smelting process. *Proceedings of the Terkel Rosenqvist Symposium*, pages 177–199.

Sun, K., Takahashi, R., and Yagi, J. I. (1992). Reduction kinetics of cement-bonded natural ilmenite pellets with hydrogen. *ISIJ international*, 32(4):496–504.

Sunde, M. (2012). Organic binder as a substitute for bentonite in ilmenite pelletization. *Norwegian University of Science and Technology, Department of Materials Science and Engineering*.

Taylor, L. A., Williams, R. J., and McCallister, R. H. (1972). Stability relations of ilmenite and ulvöspinel in the Fe-Ti-O system and application of these data to lunar mineral assemblages. *Earth and Planetary Science Letters*, 16(2):282–288.

U.S. Geological Survey (2013). Mineral commodity summaries 2013: U.S. Geological Survey.

Vijay, P. L., Venugopalan, R., and Sathiyamoorthy, D. (1996). Preoxidation and hydrogen reduction of ilmenite in a fiuidized bed reactor. *Metallurgical and Materials Transactions B*, 27(5):731–738.

Appendix A

Acronyms

ANSTO Australian Nuclear Science and Technology Organisation

EPMA Electron Probe Micro-Analysis

PCM Progressive-Conversion Model

SCM Shrinking-Core Model

TGA Thermogravimetric Analysis

XRD X-Ray Diffraction

Appendix B

EPMA Pictures.

B.1 Pellets reduced with H_2 gas

B.1.1 Mapping of Fe, Ti and O

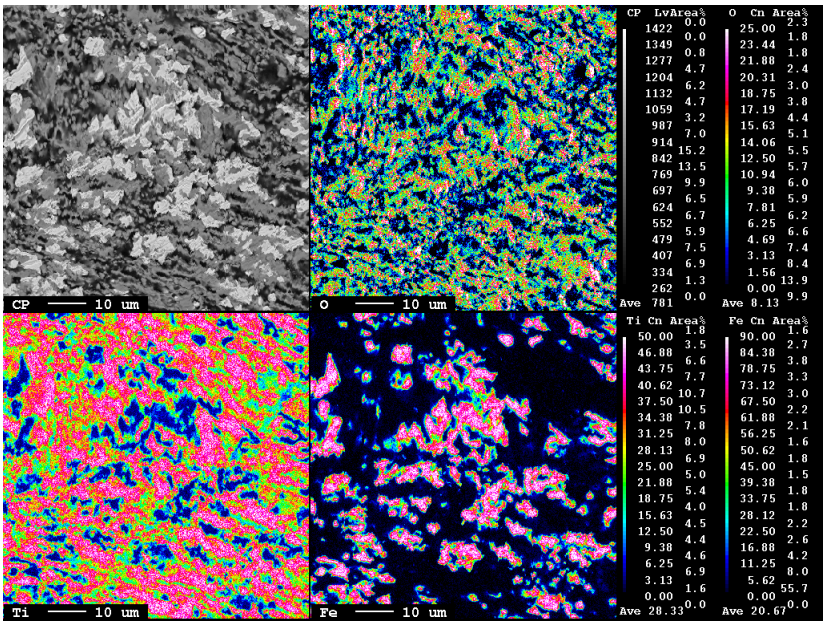

Figure B.1: Mapping of iron, titanium and oxygen in an ilmenite pellet reacted with H_2 at the surface (x2000).

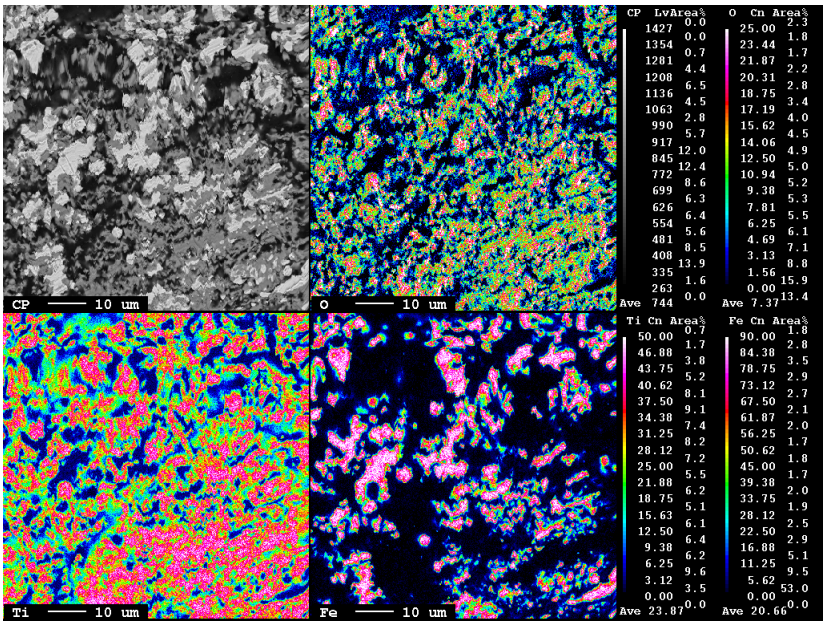

Figure B.2: Mapping of iron, titanium and oxygen in an ilmenite pellet reacted with H_2 at 2 mm deep (x2000).

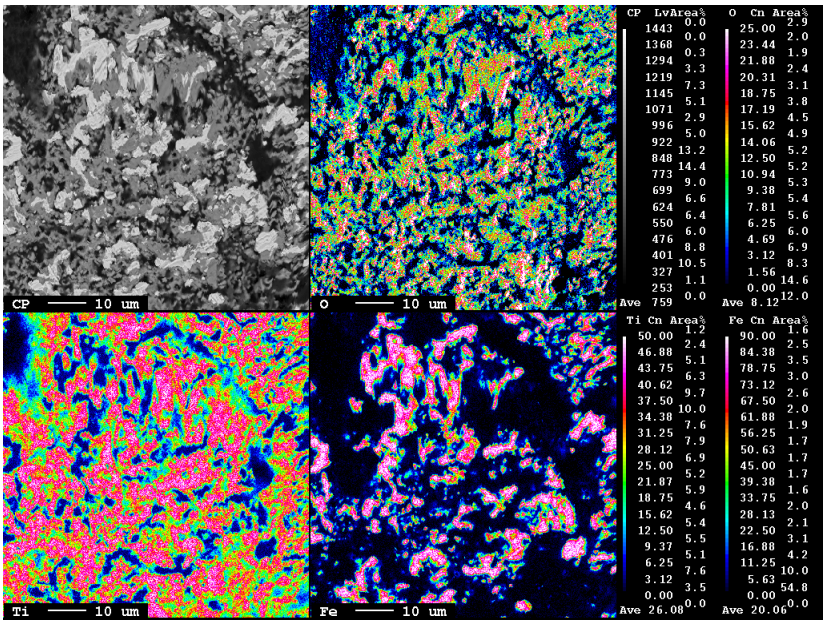

Figure B.3: Mapping of iron, titanium and oxygen in an ilmenite pellet reacted with H_2 at 4 mm deep (x2000).

B.2 Pellets reduced with CO gas

B.2.1 Mapping of Fe, Ti and O

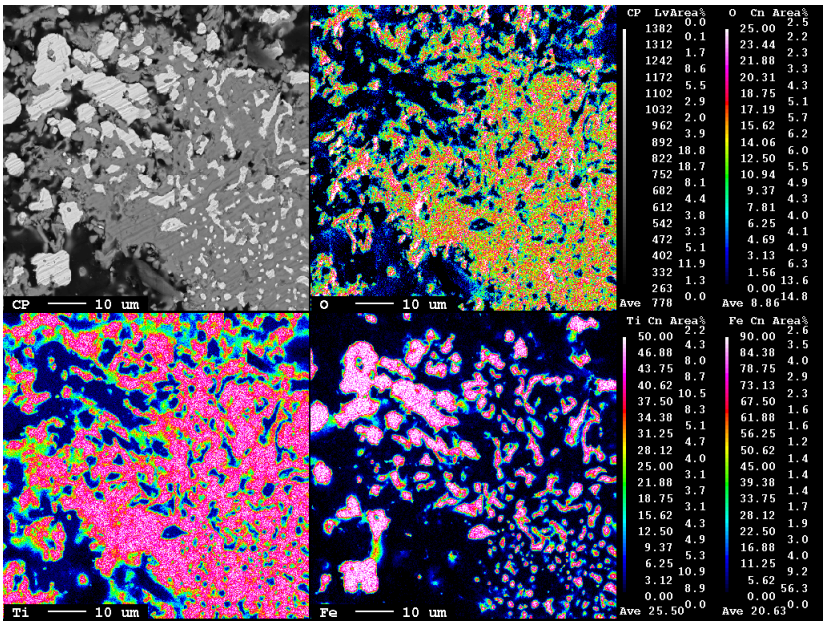

Figure B.4: Mapping of iron, titanium and oxygen in an ilmenite pellet reacted with CO at the surface (x2000).

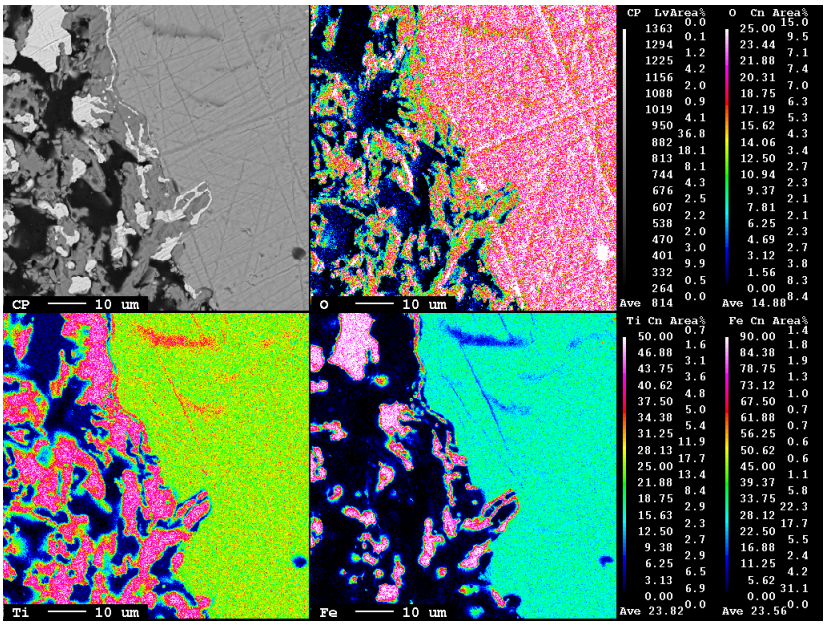

Figure B.5: Mapping of iron, titanium and oxygen in an ilmenite pellet reacted with CO at 2 mm deep (x2000).

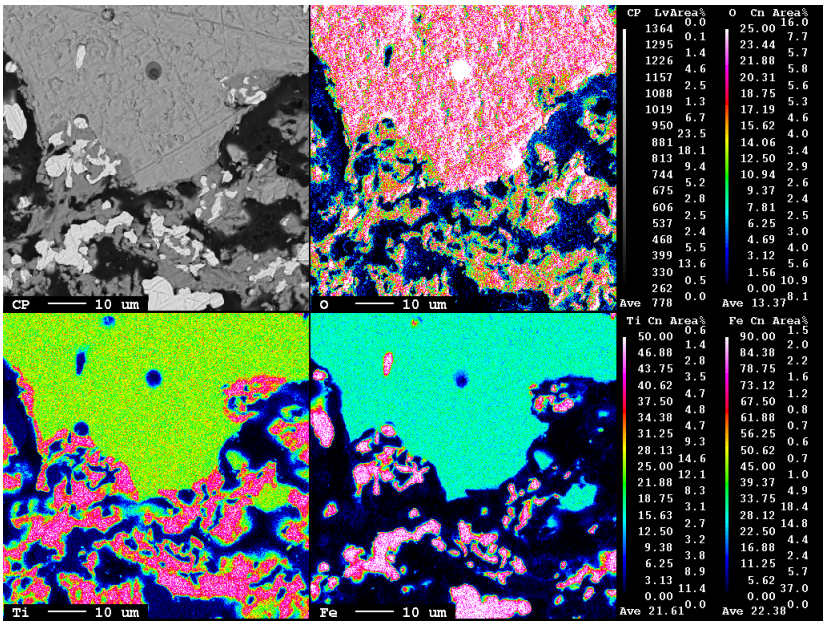

Figure B.6: Mapping of iron, titanium and oxygen in an ilmenite pellet reacted with CO at 4 mm deep (x2000).

Appendix C

Ilmenite synthesis protocol

C.1 Use of the cold crucible induction furnace

Dismount the set-up

- The first step here is to prepare the set up by positioning all the devices needed.
- Use the crank to lower the height of the crucible
- Unplug the water tubes by pulling the ring at the joint. Be careful, water is still present in the circuit, so be aware and use a container to limit the water flows.
- Remove the two intern glass tubes and the external protection sheet
- Move the crucible at the edge of the platform, to be able to remove the last glass tube. Remove the internal protection sheet
- If the boron nitride coating is good, it is now possible to prepare the set-up

Mount the Set-up

- Fill the crucible
- Place the external glass tube by the bottom of the induction coil, then place the crucible on the platform. Place the heat protection around the crucible.
- Place the external glass tube so that is protects until the bottom of the crucible

- Place the internal glass tube by the top, and place the external heat protection sheet around the external glass tube
- Plug the water tubes
- Use the crank until the glass tube touches the top, and presses the spring of about 5 mm.
- Position the spectropyrometer on its support; use the LASER ON/OFF function, on the software, for the aiming.

Evacuate the crucible atmosphere

- Empower the pressure board using "INSTR" button (figure 1B). Open the pump circuit, and close the output circuit. "DRUCK" button (figure 1A) enables the display of pressure measurement.
- Open the pump circuit (figure 2E) and close the output circuit (figure 2D).
- Enable the "Rotasjon pump" on the board (figure 1C). The pressure will start to decrease to approximately 6 -10 Pa. At this value, close the pump circuit and stop the pump. (figure 2E and 1C)

Fill the inside with Argon atmosphere

- Close the cage
- Once the bottle is connected, check that the white regulator (figure 3F) is in closed position (it is if you can rotate it easily in the two directions). Check that the output is closed.
- Open the blue regulator on the top to allow gas to enter the decompression chamber. Don't stand in front of the white regulator in case of accident.
- Open the white regulator (figure 3F) by screwing it
- Open the little output regulator (figure 4G)
- Proceed to the filling, opening full the ball regulator (figure 5H)

- Once filled, reduce to flow to 70
- Open the water circuit by turning the blue switch.

Enable and stop the induction

- Open the cooling circuit. To avoid overpressures, open “Retur” first, and then “Tur”. To close it, proceed following the same logic (“tur” first, then “retur”) (figure 6I and 6J)
- First, turn the button to “2” (figure 7K) on the electric desk.
- Put the switch to “1” on the furnace (figure 8L).
- Press PUMP button (figure 9N), and then START (figure 9O). Wait 5 minutes.
- Check that the power is down to 0
- Press RF ON and wait 1 minute before increasing the power (figure 9P).
- Increase the power to the desired level (figure 9Q). Do not overreach the 1.8 value for the ANODE (figure 9M).
- To stop, shut down RF ON and START.
- After cooling, close water circuits. Mind that overpressures must be avoided by closing “tur” first, then “retur”.
- Close gas.

C.2 Materials positionning in the crucible

To ensure a good melting, the most important parameters are the temperature and the raw material positionning. Of course, the two are heavily related. The iron material has to be placed on the top. Experiment showed that the iron is melting easier when placed concentrated. Because it goes down when melting, it is necessary to place it on the top, otherwize only the bottom materials melt. In addition, place a little of iron on the surface helps to melt all the oxides at the surface and preventing crust forming.The

rest of oxides must me placed below the iron. The second most important factor is the temperature. The 70% of power has been essential for the melting. Here, the aim is to reach a temperature high enough to melt everything, even the layer close to the cold crucible wall. Having temperatures higher than 1600°C displayed on the spectropyrometer is usually a good indicator that the melting is complete.

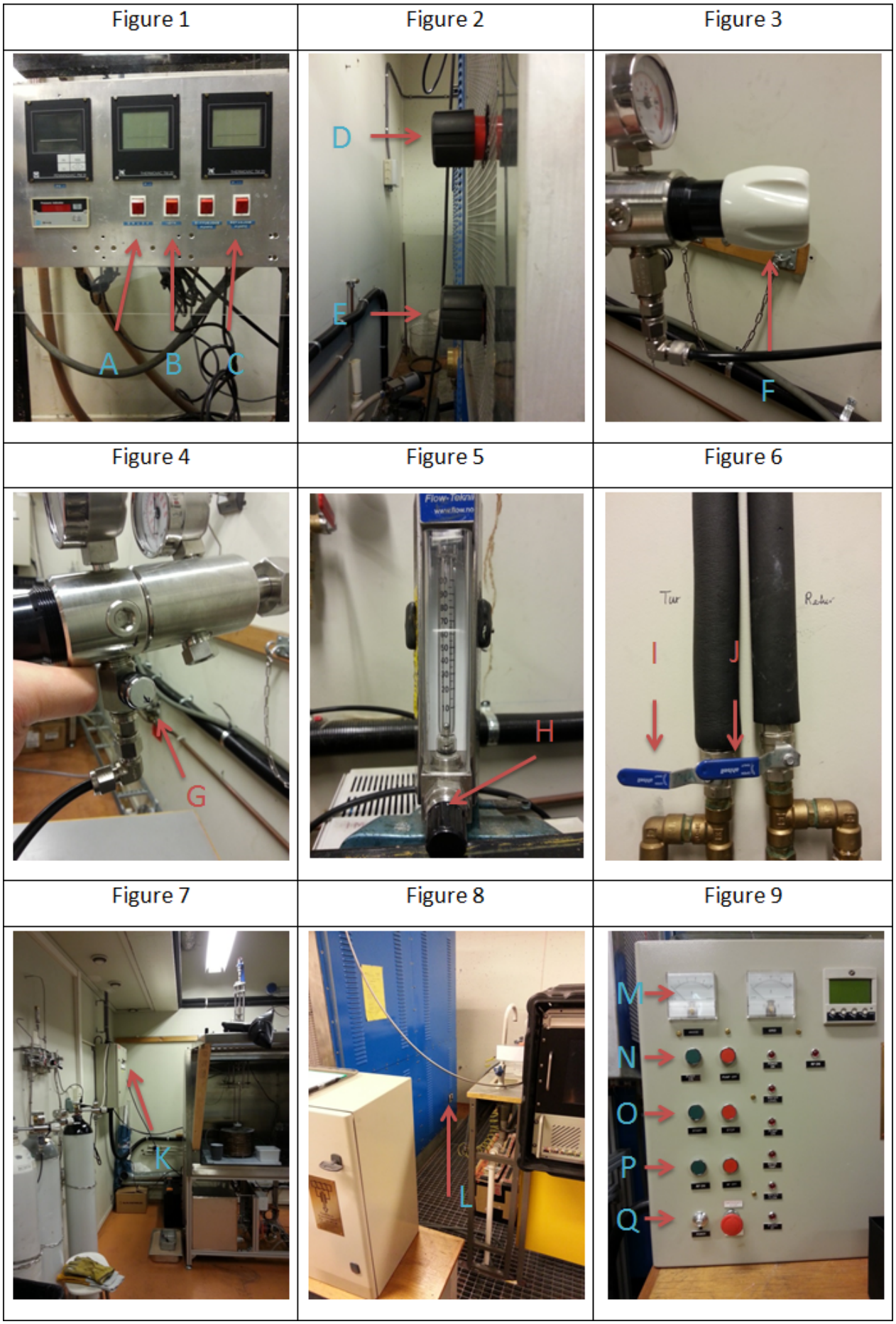

Figure C.1: Pictures of the cold crucible induction furnace and its components.